DEFENCE
SCIENCE & TECHNOLOGY

A Parametric Study of Jet/Vortex Interactions in the AMRL Water Tunnel

Lincoln P. Erm

DSTO-TR-1209

12

DEFENCE
SCIENCE & TECHNOLOGY

A Parametric Study of Jet/Vortex Interactions in the AMRL Water Tunnel

Lincoln P. Erm

Air Operations Division
Aeronautical and Maritime Research Laboratory

DSTO-TR-1209

ABSTRACT

In this report, details are given of a parametric study undertaken in the AMRL flow-visualisation water tunnel to determine how vortices are affected when they interact with different types of jet flows. The effects on vortices of jets having different shapes, velocities, locations and pitch angles were investigated. The flow was visualized using dye and vortex behaviour was examined for 42 different jets. It was found that jet shape, jet velocity and jet location all had a significant effect on vortex behaviour, whereas jet pitch angle generally had a minimal effect. Possible physical explanations for vortex behaviour have been proposed. The parametric study is the first stage of a longer investigation aimed at determining the best jet configurations to use to control vortical flow over modern high-performance aircraft to improve aircraft control at extreme flight attitudes. The findings of the initial parametric study will be used in any ongoing work on the investigation.

Published by

DSTO Aeronautical and Maritime Research Laboratory
506 Lorimer St
Fishermans Bend, Victoria 3207 Australia

Telephone: (03) 9626 7000
Fax: (03) 9626 7999

AR- 012-017
September 2001

APPROVED FOR PUBLIC RELEASE

A Parametric Study of Jet/Vortex Interactions in the AMRL Water Tunnel

Executive Summary

Modern combat aircraft such as the F/A–18 exploit low-pressure vortical flows over the aircraft to obtain enhanced performance at extreme flight attitudes. If the vortical flow is modified so that the controlling forces and moments on the aircraft are changed favourably, then aircraft performance and control can be improved. Many techniques for doing this have been proposed by researchers over the years. One such technique for modifying the vortical flow is to use jet flows, which interact with the vortices. At AMRL, an investigation has commenced to determine the best jet configurations to use to control the vortical flow. The investigation has been broken down into a number of stages and the first stage is described in this report.

Details are given of a parametric study undertaken in the AMRL flow-visualization water tunnel to determine how vortices are affected by different types of jet flows. A nominally-constant vortex was produced along the test section using a thin cambered plate and different jets were produced by pumping water through jet nozzles. The parameters investigated were jet shape, jet velocity, jet location and jet pitch angle. The tunnel free-stream velocity used was 0.1 m/s. Jet nozzles having circular and rectangular outlets were tested and three different jet outlet velocities were used, namely 0.4, 0.8 and 1.2 m/s. Jets were located on both sides of the vortex and at different angles to the vortex. The flow was visualized using dye and vortex behaviour was examined for 42 different jets. In each case the lateral displacement of the vortex core, resulting from the interaction with the jets, was measured for a range of longitudinal positions. It was found that jet shape, jet velocity and jet location all had a marked effect on vortex behaviour, whereas jet pitch angle generally had a minimal effect. Possible physical explanations for vortex behaviour have been proposed.

For the next stage of the investigation, it is planned to carry out jet/vortex flow-visualization experiments in the water tunnel using a generic model of a high-performance aircraft to produce the jets and the vortices. Jet flows will be produced by water flowing through ducts from the high-pressure side to the low-pressure side of aircraft lifting surfaces away from the forebody of the aircraft. The interaction between the aircraft vortices and the jet flows will be examined in an attempt to determine the jet/vortex cases most likely to improve aircraft control at extreme flight attitudes. The findings of the initial parametric study, referred to above, will be used as a guide when setting up the experimental program so that only the important jet cases are tested.

Author

Lincoln P. Erm
Air Operations Division

Lincoln Erm obtained a Bachelor of Engineering (Mechanical) degree in 1967 and a Master of Engineering Science degree in 1969, both from the University of Melbourne. His Master's degree was concerned with the yielding of aluminium alloy when subjected to both tensile and torsional loading. He joined the Aeronautical Research Laboratories (now called the Aeronautical and Maritime Research Laboratory) in 1970 and has worked on a wide range of research projects, including the prediction of the performance of gas turbine engines under conditions of pulsating flow, parametric studies of ramrocket performance, flow instability in aircraft intakes and problems associated with the landing of a helicopter on the flight deck of a ship. Concurrently with some of the above work, he studied at the University of Melbourne and in 1988 obtained his Doctor of Philosophy degree for work on low-Reynolds-number turbulent boundary layers. Lincoln is currently employed as a Research Scientist and is undertaking research investigations in the low-speed wind tunnel and the water tunnel.

Contents

Notation

D	Jet diameter ($D = 6.4 \times 10^{-3}$ m for the circular jet)
r	Distance from the centre of a vortex core to a point in a vortical flow field (m)
R_{CF}	Reynolds number of the cross-flow ($R_{CF} = U_{CF}D/\nu$)
R_J	Reynolds number of a jet ($R_J = U_J D/\nu$)
U_{CF}	Velocity of the cross flow in the water tunnel, (m/s)
U_I	Induced circumferential velocity in a vortical flow field, (m/s)
U_J	Jet velocity at the nozzle outlet, (m/s)
$x_J y_J z_J$	Jet coordinate system (right-handed)
$x_T y_T z_T$	Tunnel coordinate system (right-handed)
x_J, y_J, z_J	Distances or directions in the jet coordinate system, (m)
x_T, y_T, z_T	Distances or directions in the tunnel coordinate system, (m)
Δ_H	Lateral displacement of the core of a vortex in the horizontal direction, (mm)
Δ_V	Lateral displacement of the core of a vortex in the vertical direction, (mm)
ν	Kinematic viscosity of water ($\nu = 1.011 \times 10^{-6}$ m^2/s for water at 20° C)
θ	Pitch angle of the jet, (degrees)
Γ	Strength or circulation of a vortex, (m^2/s)
ϕ	Roll angle of the jet, (degrees)
ψ	Yaw angle of the jet, (degrees)
cvj	Contra-vortex jet
pvj	Pro-vortex jet

1. Introduction

Modern combat aircraft such as the F/A–18 exploit vortical flows over the aircraft to obtain enhanced performance at extreme flight attitudes. The vortex system is primarily made up of vortices emanating from the forebody of an aircraft and from the highly-swept wings and wing strakes. The low pressures in the cores of these vortices create "vortex lift", which when combined with conventional aircraft lift enables aircraft to generate meaningful lift at high angles of incidence and this improves aircraft manoeuvrability and controllability when operating at extreme attitudes.

If the vortical flow around the aircraft is modified so that the controlling forces and moments on the aircraft are changed favourably then aircraft performance and control can be further improved. Many techniques for doing this have been proposed by researchers and the modification of aircraft vortical flows can be classified into two categories, namely (1) modification of the vortical flow near the forebody and (2) modification of the vortical flow downstream of the forebody. The first category includes modification of vortices by blowing air through nozzles or slots in the forebody, by sucking air through slots or holes near the forebody tip, by using sharp-edged strakes attached to the forebody and by manipulation of the shape of the extreme nose of the forebody. The second category includes modification of vortices by blowing air over wings or strakes and by using deployable surfaces at strategic locations away from the forebody, such as at the junction of the strake and the wing leading-edge on aircraft with straked wings.

It has also been shown that the flow of air through vents and ducts from the high-pressure side to the low-pressure side of aircraft lifting surfaces away from the forebody can modify vortical flows and affect aircraft performance and control. In their study into the effects of passive jet flows on the performance of an F/A–18E aircraft at extreme flight attitudes, Shah & Clemons (1995) showed that aircraft performance could be improved significantly by small configuration changes in the size and shape of the flow-through vent between the leading-edge extension and the inboard leading-edge flap. Walker (1993) suggested that an uncommanded roll and yaw in an F–15 aircraft at a high angle of attack ("Bitburg manoeuvre") was largely due to the interaction between wing root vortices and air from the aircraft's gun gas purging system.

The use of such duct jet flows to modify vortical flows over modern combat aircraft is potentially a technique for aircraft control at extreme flight attitudes. This technique could be implemented using minimal hardware and there would be little interference with existing aircraft systems, unlike blowing techniques used for the control of vortices near the forebody, which often require the installation of substantial hardware in the nose of the aircraft. The chosen technique might only rely on the flow between the surfaces that occurs due to normal pressure differences.

The effects of duct jet flows on vortex flows and the application of such effects for aircraft control purposes is currently being investigated at AMRL and the first stage of the study is described in this report.

Details are given of a parametric study undertaken in the AMRL flow-visualization water tunnel to determine how vortices are affected by different types of jet flows. A standard baseline vortex was produced using a thin cambered plate having a profile of half of a NACA 0012 aerofoil section. Different jets were produced by pumping water through jet nozzles. Circular and rectangular jets were used and jet velocity, jet location, jet pitch angle, (for the circular jet) and jet roll angle (for the rectangular jet) were varied. The flow was visualized using dye. The effects of the different jets on the vortex were determined by measuring the lateral displacement of the vortex for a range of longitudinal positions. The findings of the initial study, given in this report, will be used as guidelines when determining the best way to modify vortical flows in future work on aircraft control.

2. Representation of Jet and Vortex Flows

When a jet discharges normal to a cross-flow, the interaction between the two flows causes the jet to deflect in the direction of the cross-flow and a complicated system of jet vortices is formed. According to Fric (1990) and Fric & Roshko (1991), four types of coherent structure can be discerned in the near field of a circular jet. These structures, shown in Figure 1 (see Fric & Roshko, 1994), are (1) the jet shear layer vortices around the circumference of the bending jet, (2) the nascent counter-rotating vortex pair, (3) a system of horseshoe vortices on the cross-flow wall and (4) a system of wake vortices extending from the wall to the jet. The near field is defined somewhat arbitrarily to include the first few jet diameters of the flow, where most of the jet's bending occurs and where the cross-flow/jet interaction dynamics is the most complex (Fric & Roshko, 1991). Scorer (1958) appears to be amongst the first researchers to draw attention to the existence of counter-rotating vortices in a transverse circular jet and he indicated that the vortices occur as a result of the impulse of the jet on the cross flow. He proposed that the vortices were formed from the roll up of the vorticity at the sides of a round hole. The vortices at the leading and trailing edges of the hole were considered to annul each other. The jet shear-layer vortices dominate the near field of the jet, but as the jet develops, the counter-rotating pair of vortices assume a characteristic kidney shape and these vortices dominate the jet structure in the far field. The current investigation is only concerned with the far field of the jets.

A diagrammatic representation of a vortex and a pro-vortex circular jet (see Section 3.4) is given in Figure 2. The figure depicts the general flow directions within the jet and the vortex when each is considered in isolation, i.e. no interaction between the vortex the jet. The diagram is for a circular jet discharging normal to the cross flow, but other jets, such as rectangular jets, can have different vortical structures.

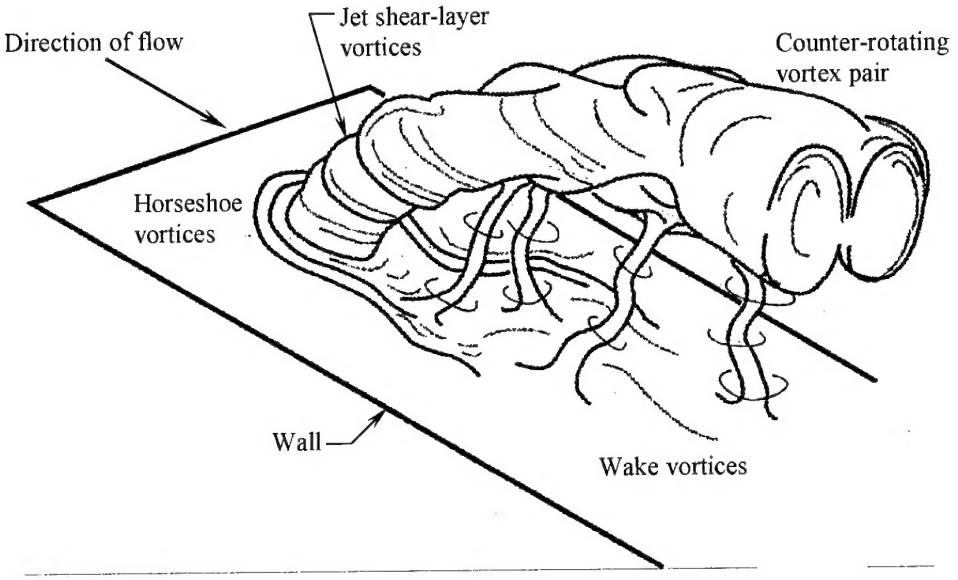

Figure 1. Representation of vortical structures associated with the transverse-jet near-flow field (based on a diagram given by Fric & Roshko 1994).

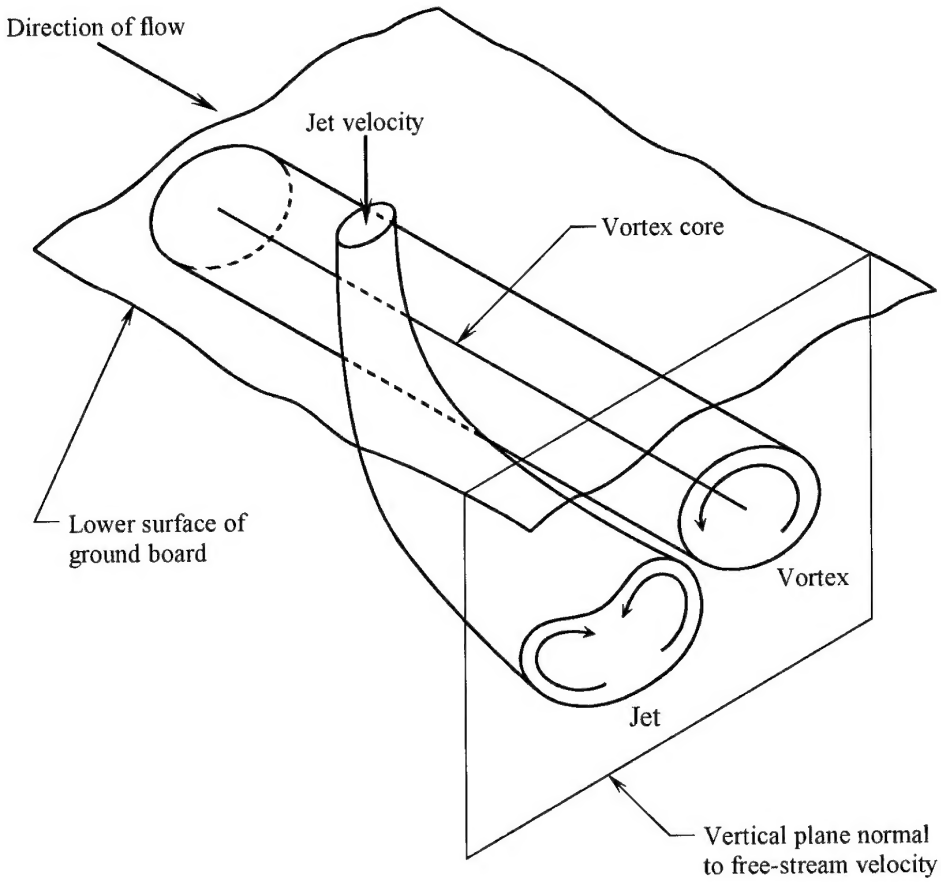

Figure 2. Diagrammatic representation of a vortex and a pro-vortex jet.

3. Details of Experiments

3.1 Water Tunnel and Associated Facilities

The jet/vortex experiments were carried out at AMRL in an Eidetics[1] Model 1520 flow-visualization water tunnel shown diagrammatically in Figure 3. The tunnel has a horizontal-flow test section 1520 mm long, 510 mm deep and 380 mm wide and is constructed so that it is possible to look directly upstream into the test section from a window at the end of the diffuser. The free-stream velocity can be varied between 0 and 0.6 m/s. There are six dye canisters on the tunnel that can be pressurised with air to force dye through tubes to selected locations on a model for flow-visualization studies. The flow rate of dye in each circuit can be controlled independently using adjustable valves. There is also a suction/blower pump on the tunnel that can be used to suck water into an orifice or to blow water out of an orifice. The mass flow rate of water through the pump can be varied between 0 and approximately 88 mL/s.

3.2 Vortex and Jet Apparatus

The apparatus used to generate the vortices and the jets in the experiments is shown diagrammatically in Figure 4.

3.2.1 Vortex Apparatus

A vortex was generated from the tip of a thin cambered plate, mounted vertically in the test section with its base downward, rather than with its base upward or near a side wall, so that the wake from the main body of the plate had minimal effect on the jet/vortex interaction. To obtain a vortex suitable for the current experiments, it was necessary to test several different designs of cambered plate over a range of pitch angles and tunnel free-stream velocities. The selected cambered plate was formed by bending aluminium plate (1.55 mm thick) to follow the profile of the low-pressure or leeward side of a NACA 0012 aerofoil section, having a chord of 253 mm and a span of 120 mm. The cambered plate was attached to a base plate, having a profile of a NACA 0012 aerofoil section, which in turn was mounted on a support, as shown in Figure 4. To obtain a suitable vortex, the base plate was set at a pitch angle of 12°, and the nominal tunnel free-stream velocity used was 0.1 m/s. It was also necessary to cut away the nose portion of the cambered plate, corresponding to about 1% of its chord length, so that the effective pitch angle of the plate was about 13.3°. The plate was cut to remove a region of reversed flow that existed immediately downstream of the nose of the uncut plate. The reversed flow caused the vortex to be unsteady, making it unsuitable for the investigation. The core and the outer-flow region of the vortex were visualized using fluorescein sodium dye emitted from ports strategically located on the plate. Hypodermic tubes, used to form the dye ports, were glued to the concave side of the

[1] Eidetics Corporation, 3425 Lomita Boulevard, Torrance, CA, 90505, USA.

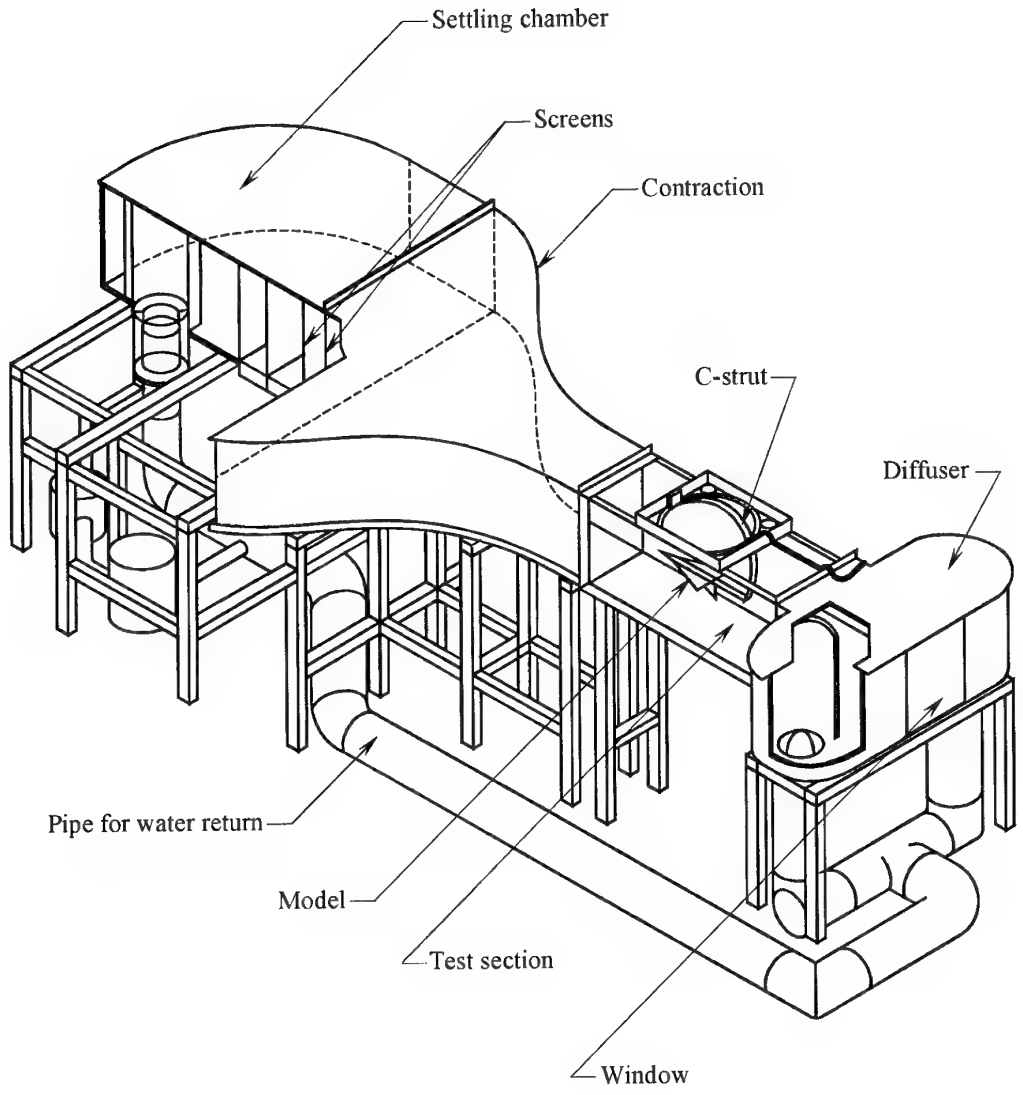

Figure 3. Diagrammatic representation of the Eidetics Model 1520 flow-visualization water tunnel.

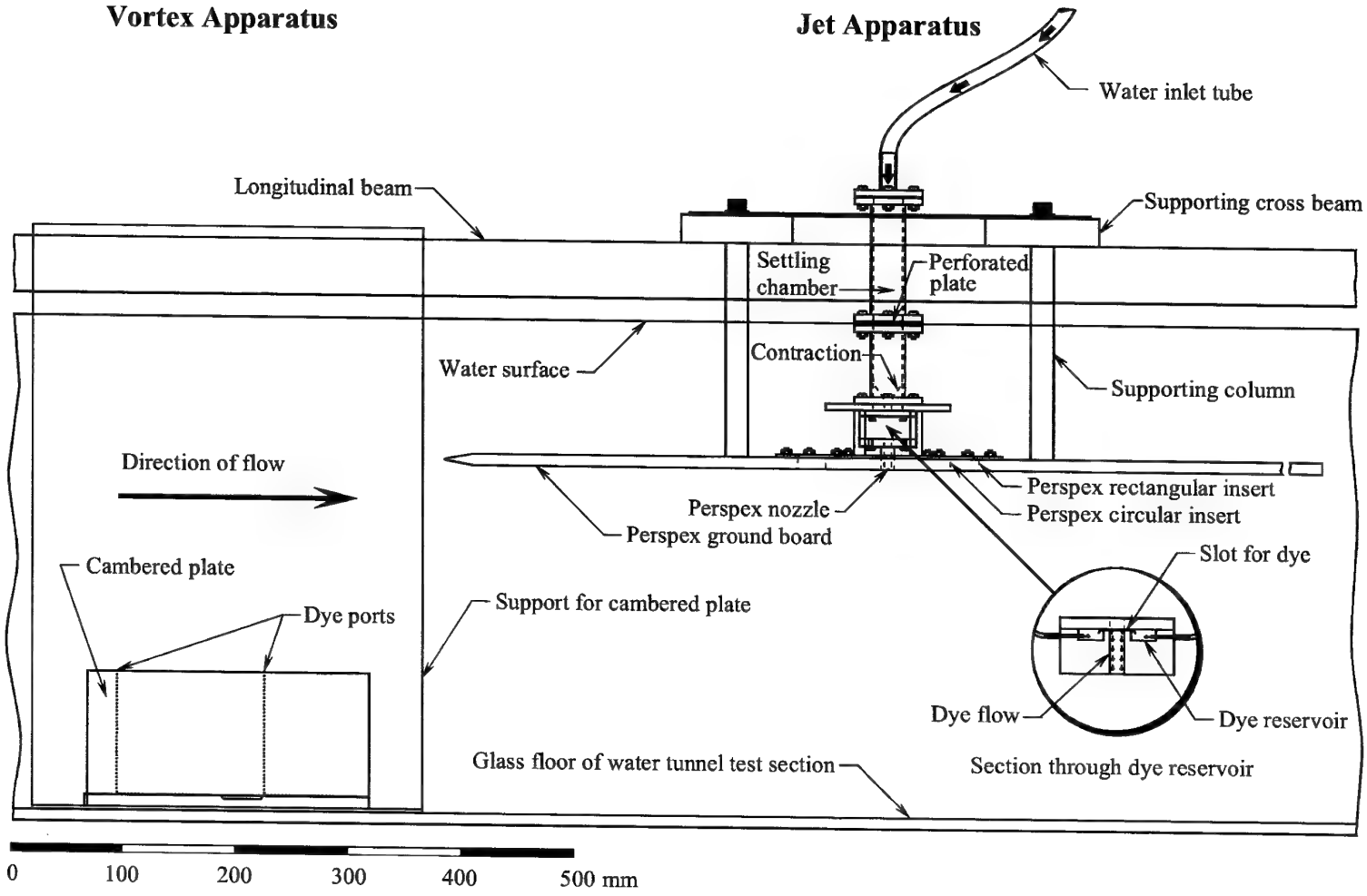

Figure 4. Diagrammatic representation of the vortex apparatus and the jet apparatus; (a) side view.

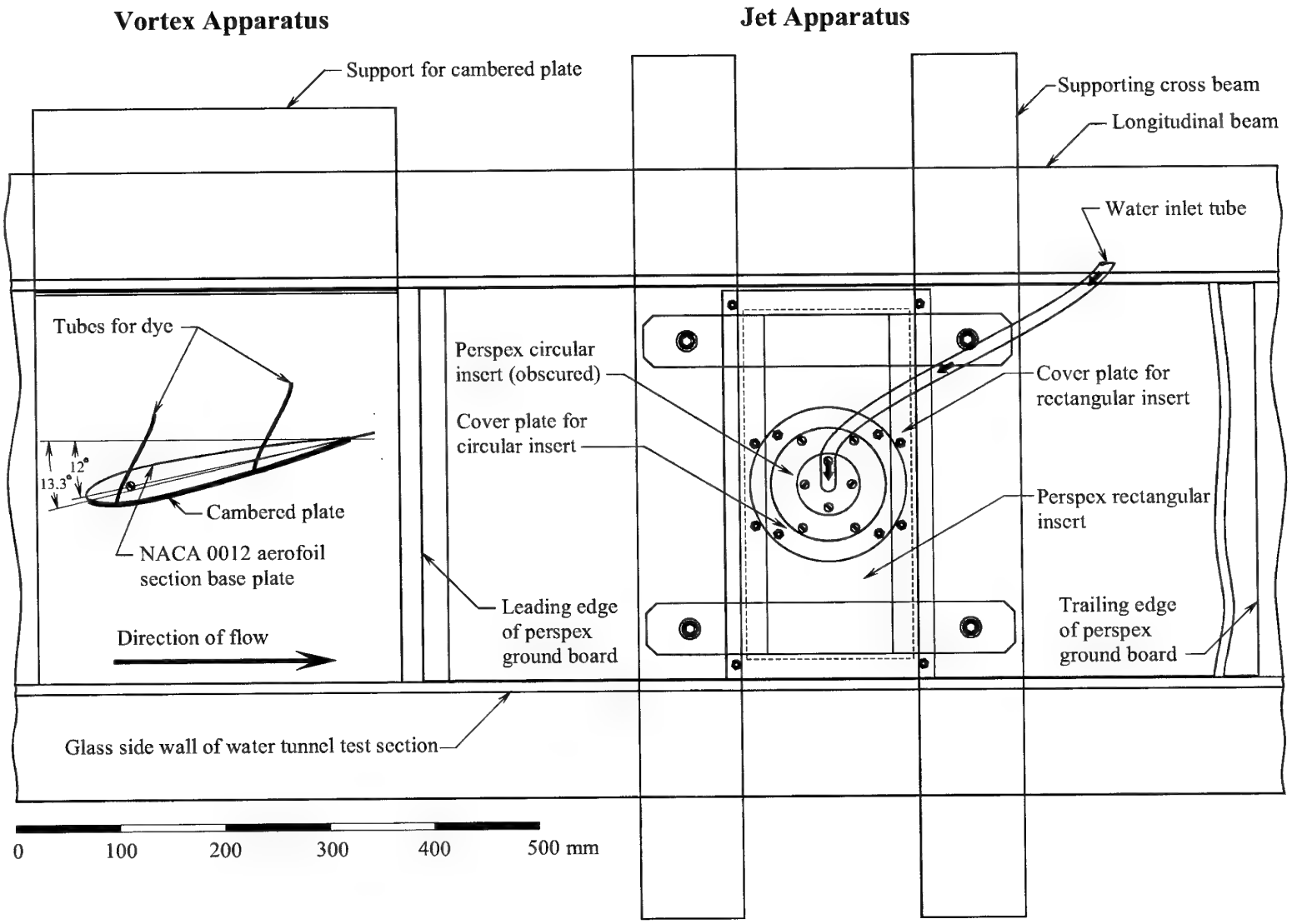

Figure 4 cont'd. Diagrammatic representation of the vortex apparatus and the jet apparatus; (b) plan view.

plate at chordwise distances of 27 and 162 mm from the location of its original leading edge. The vortex apparatus could be raised or lowered in the tunnel as required to adjust the height of the vortex. The cambered plate was positioned laterally on its support so that the core of the unperturbed vortex passed directly under the origin of the tunnel coordinate system (see Section 3.3).

The vortex rotated in an anti-clockwise direction when viewed looking upstream. Measurements indicated that the velocity of the core of the vortex was about 4% slower than the tunnel free-stream velocity between reference markers on the ground board, located 600 mm apart (see Section 3.6). The vortex remained stable to the end of the tunnel and its core was acceptably straight over the length of the ground board. This is consistent with the findings of Jacob, Liepmann & Savas (1995), who carried out experiments in a towing tank and found that the trailing vortices from a NACA 0012 rectangular aerofoil were generally steady and stable for at least a distance of 250 spans downstream of the aerofoil.

3.2.2 Jet Apparatus

The jet apparatus, shown in Figure 4, was constructed by modifying existing AMRL equipment. Components forming the water-flow circuit are mounted on a perspex ground board which is supported in the tunnel test section using columns and cross beams as shown. The suction/blower pump (see Section 3.1) pumps water into a settling chamber, through a perforated plate, through a contraction, past a dye slot, through a circular or rectangular nozzle located in the ground board and then into the tunnel cross-flow. A section through the dye reservoir is shown as an inset in Figure 4. Fluorescein sodium dye was pumped into the dye reservoir and through a slot of depth 0.1 mm to mix with the jet boundary layer, thereby enabling the jet flow to be observed. The arrangement of the dye slot is similar to that used by Kelso, Lim & Perry (1996). The ground board is 1183 mm long and 384 mm wide and the gap between the sides of the ground board and the vertical walls of the tunnel varies between 0 and about 4 mm (the vertical walls of the tunnel diverge slightly in the direction of flow to allow for boundary-layer growth). For the current experiments, the ground board was positioned in the tunnel so that its leading edge was 550 mm downstream of the inlet of the test section of the tunnel. A rectangular hole of dimensions 340 mm by 160 mm has been machined in the ground board to accommodate interchangeable rectangular inserts. The components forming the water-flow circuit are attached to these inserts and the nozzles can be positioned at 17 different lateral positions on the ground board, as shown in Figure 5, by using different inserts. Figure 4 shows the apparatus configured to produce jet flows perpendicular (initially) to the direction of the cross-flow, but the apparatus can also be set up using an inclined nozzle having a circular outlet to produce jet flows inclined at 45° (initially) upstream or downstream. The two circular nozzles have an outlet of diameter 6.4 mm and the rectangular nozzle has outlet dimensions of 11.2 mm by 2.9 mm, so that the nozzle outlet areas of the circular and rectangular jets are equal to within 1.0%. The columns supporting the ground board are interchangeable to enable the ground board to be raised or lowered as required. The lower side of the ground board was positioned about 80 mm below the surface of the water for the current study.

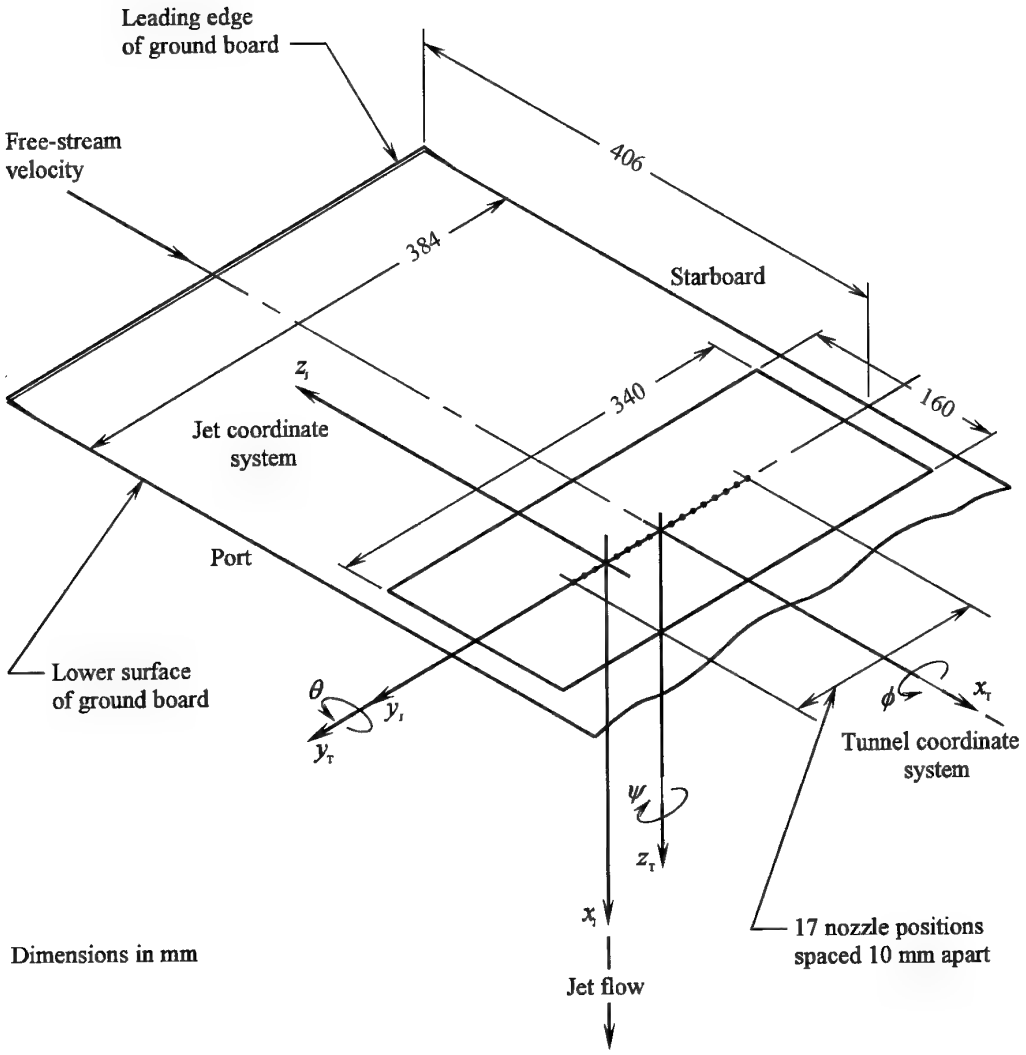

Figure 5. Lower surface of the ground board showing the tunnel and the jet coordinate systems.

3.3 Coordinate Systems

For the purpose of the current study, the tunnel coordinate system, $x_T y_T z_T$, has its origin located at the intersection of the lower surface of the ground board and the jet longitudinal axis, when the jet is at its central location in the ground board, as shown in Figure 5. The x_T axis is horizontal and is positive in the direction of the free-stream velocity, the y_T axis is horizontal and is positive to the port side (defined in Figure 5) of the tunnel and the z_T axis is positive vertically downwards. The axes form a right-handed orthogonal coordinate system and remain fixed with respect to the ground board and the tunnel.

For each of the nozzles, the jet coordinate system, x_J y_J z_J, has its origin located at the intersection of the nozzle longitudinal centreline and the exit plane of the nozzle, which coincides with the lower surface of the ground board. The axes form a right-handed orthogonal coordinate system that remains fixed with respect to the nozzle. The position of the origin of the jet coordinate system is not fixed relative to the origin of the tunnel coordinate system, but can be located at any of the 17 positions shown in Figure 5, depending on where the nozzle is positioned laterally in the ground board. The directions of the x_J, y_J and z_J axes can vary, depending on the nozzle configuration used, but the x_J axis is always along the nozzle longitudinal centreline and is positive in the direction of the jet flow at the nozzle outlet. For the rectangular nozzle, the y_J and z_J axes are parallel to the 2.9 mm and 11.2 mm sides respectively of the rectangular outlet. The jet coordinate system shown in Figure 5 is for a jet having a flow perpendicular (initially) to the tunnel free-stream velocity and located 50 mm to port of the tunnel coordinate system.

In Figure 5, the angles that rotate the tunnel axes, x_T, y_T and z_T, so that they are parallel to, and in the same direction as, corresponding jet axes, x_J, y_J and z_J, are referred to as the yaw angle, ψ, the pitch angle, θ, and the roll angle, ϕ. The positive directions of ψ, θ and ϕ conform to the conventional right-hand screw rule about the relevant axes. For the tunnel and jet coordinate systems shown in Figure 5, $\psi = 0°$, $\theta = -90°$ and $\phi = 0°$.

3.4 Details of Vortex and Jets

Details of the vortex and the jets used in the experiments are given below –nominal flow conditions are quoted. The different jets are described in terms of four parameters: jet shape, jet velocity, jet location and jet pitch angle.

- **Vortex:**

The unperturbed vortex was produced using part of a NACA 0012 aerofoil section set at a pitch angle of 12° and the tunnel free-stream velocity was 0.1 m/s (see Section 3.2.1). The unperturbed vortex was nominally the same for the different jet/vortex cases and it passed through a point directly below the origin of the tunnel coordinate system, namely $x_T = 0$, $y_T = 0$ and $z_T = 73$ mm.

- **Jet shape:**

Nozzles having a circular outlet of diameter 6.4 mm and a nozzle having a rectangular outlet with dimensions of 11.2×2.9 mm were used. The circular nozzles and the rectangular nozzles had cross sectional flow areas of 32.17 and 32.48 mm^2 respectively. The rectangular nozzle was used at four roll angles, namely $\phi = 0°$, 45°, 90° and 135°, and the rectangular jets at the different roll angles are categorised as four different jet shapes when presenting data.

- **Jet velocity:**

Three different jet outlet velocities were used, namely $U_J = 0.4$, 0.8 and 1.2 m/s, corresponding to velocity ratios, U_J/U_{CF}, of 4, 8 and 12 respectively, for both the circular and the rectangular jets. The jet velocities were in fact mean jet velocities, calculated using the mass flow rates through the nozzles and the cross-sectional areas of the nozzles.

- **Jet location:**

The origin of the jet coordinate system for the circular and rectangular nozzles was located at either $x_T = 0$, $y_T = 50$ and $z_T = 0$ mm, i.e. the jet was located 50 mm to port of an unperturbed vortex ($x_T/D \approx 7.5$), or $x_T = 0$, $y_T = -50$ and $z_T = 0$ mm, i.e. the jet was located 50 mm to starboard of an unperturbed vortex. The main vortex from the aerofoil rotates in an anti-clockwise direction when viewed looking upstream. For jets located on the port side of the vortex, the jet velocity in the vicinity of the nozzle outlet is in the same direction as the vortex circumferential velocity, i.e. the jets are pro-vortex jets, and conversely for jets located on the starboard side of the vortex, i.e. the jets are contra-vortex jets[2].

- **Jet pitch angle:**

Three different jet pitch angles were used for the circular jet, namely $\theta = -45°$, $-90°$ and $-135°$, and one jet pitch angle was used for the rectangular jet, namely $\theta = -90°$.

The complete experimental program comprised 18 different jet/vortex cases for the circular jets, i.e. 1 (vortex) × 1 (jet shape) × 3 (jet velocities) × 2 (jet locations) × 3 (jet pitch angles), and 24 different jet/vortex cases for the rectangular jets, i.e. 1 (vortex) × 4 (jet shapes) × 3 (jet velocities) × 2 (jet locations) × 1 (jet pitch angle).

The above jet parameters were thought to be the main ones affecting vortical flow, but vortices may also be influenced by other jet parameters not considered in the investigation, such as jet size and jet pulsating frequency.

3.5 Jet and Cross-Flow Reynolds Numbers

The Reynolds number of a jet, R_J, is given by $R_J = U_J D/\nu$, where U_J is the jet velocity, D is a jet diameter and ν is the kinematic viscosity of water. The value of D for the circular jet is 6.4×10^{-3} m. The rectangular jet has about the same flow cross-sectional area as the circular jet, so it is reasonable to use this value of D as the length scale when computing Reynolds numbers for the rectangular jet. The value of ν is 1.011×10^{-6} m²/s (for water at 20°C). For $U_J = 0.4$, 0.8 and 1.2 m/s, the approximate values of R_J are 2500, 5000 and 7500 respectively. According to Ligrani & Schwartz (1990), if jet Reynolds numbers at the jet outlet exceed 6000, then the injected fluid is fully turbulent, which is the case for $U_J = 1.2$ m/s.

The Reynolds number of the cross flow, R_{CF}, is given by $R_{CF} = U_{CF} D/\nu$, where U_{CF} is the velocity of the cross flow. For $U_{CF} = 0.1$ m/s, the approximate value of R_{CF} is 630.

3.6 Measurement of Displacement of Vortices for Different Jets

Vortex lateral displacements resulting from the jet/vortex interactions were measured to determine the effects of the different jets on the vortex. It was simpler and more

[2] The terms "upwash" and "downwash", although often used in the literature when discussing vortical transverse velocities, are not used in this report to avoid confusion. "Upwash", meaning vortical transverse flow away from a surface, is actually downwards in the current study and vice-versa for "downwash"

accurate to determine the displacement of the core of the vortex for the different jets, rather than to determine the displacement of the vortex as a whole. When measuring vortex lateral displacements, dye was therefore used to visualize only the core of the vortex. Using dye to visualize the outer-flow regions of the vortex and the jet may have obscured the behaviour of the core. The lateral displacements of the core of the vortex are denoted by Δ_V and Δ_H for the z_T (vertical) and y_T (horizontal) directions respectively.

Vortex cores were observed using two CCD video cameras, one located at the side the tunnel and the other located under the tunnel. Using "Image-Pro Plus"© Micro-Imaging computer software, three digitised images of the side view and three images of the plan view of the core of an unperturbed vortex (jet not flowing) were snapped at 8 s intervals. The three images were then superimposed to produce single side-view and plan-view images each containing three core traces. Although each unperturbed vortex was nominally the same for the different jet cases, images were acquired of unperturbed cores for each jet case to account for any slight variations in the vortical flow that may have occurred throughout the course of the investigation. The above procedure was repeated for the corresponding perturbed vortex (jet flowing). Typical images of unperturbed and perturbed vortex cores are shown in Figures 6 and 7 respectively. The perturbed cores shown in the side and plan views in Figure 7 are for the same jet case.

A computer drawing program was used to superimpose a rectangular grid on each image, as shown in Figures 6 and 7. The size of the superimposed grid was the same for all such images. Each cell in the grids was 50 mm long in the x_T direction and the overall length of the grid in the x_T direction was 600 mm. If required, the images (but not the grid) for the different cases were enlarged or reduced and/or moved so that reference marks on the ground board of the jet apparatus matched the grid at selected locations. This ensured that all images were the same size, which simplified the processing of the data. Without the adjustments, images may have varied in size if the video cameras had been moved or their zoom settings had been altered throughout the course of the investigation. Distances between base lines and the unperturbed cores were measured along grid ordinates, and likewise for perturbed cores, as shown in Figures 6 and 7 respectively. For locations where the cores for the three images coincided, only a single distance was measured at each x_T location. In cases where the cores remained substantially intact, but deviated between the three snaps, three distances were measured at x_T locations and average distances were then calculated. In regions where the jet destroyed the cores, as shown for a typical jet case in Figure 8, it was not possible to measure distances to cores. Inaccuracies in measured core displacements would have occurred due to parallax effects, i.e. vortices are generally not located in the plane of a grid, but such inaccuracies are likely to be small and would not have a significant effect on trends in vortex behaviour for the different jet cases. Values of Δ_V and Δ_H for different values of x_T were determined by evaluating the differences in the distances to cores of the perturbed and corresponding unperturbed vortices.

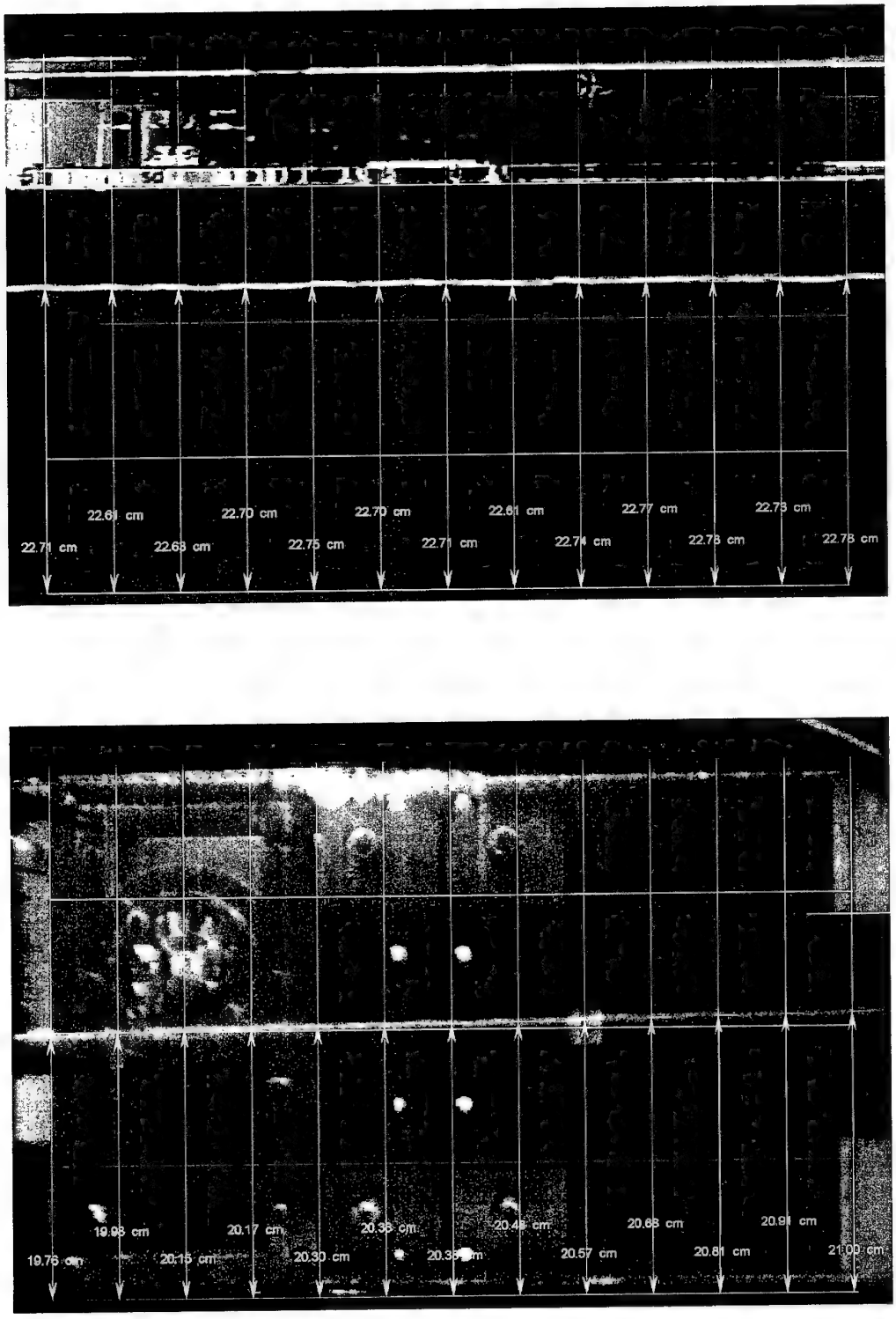

Figure 6. Typical images of cores of unperturbed vortices: (a) side view; (b) plan view.

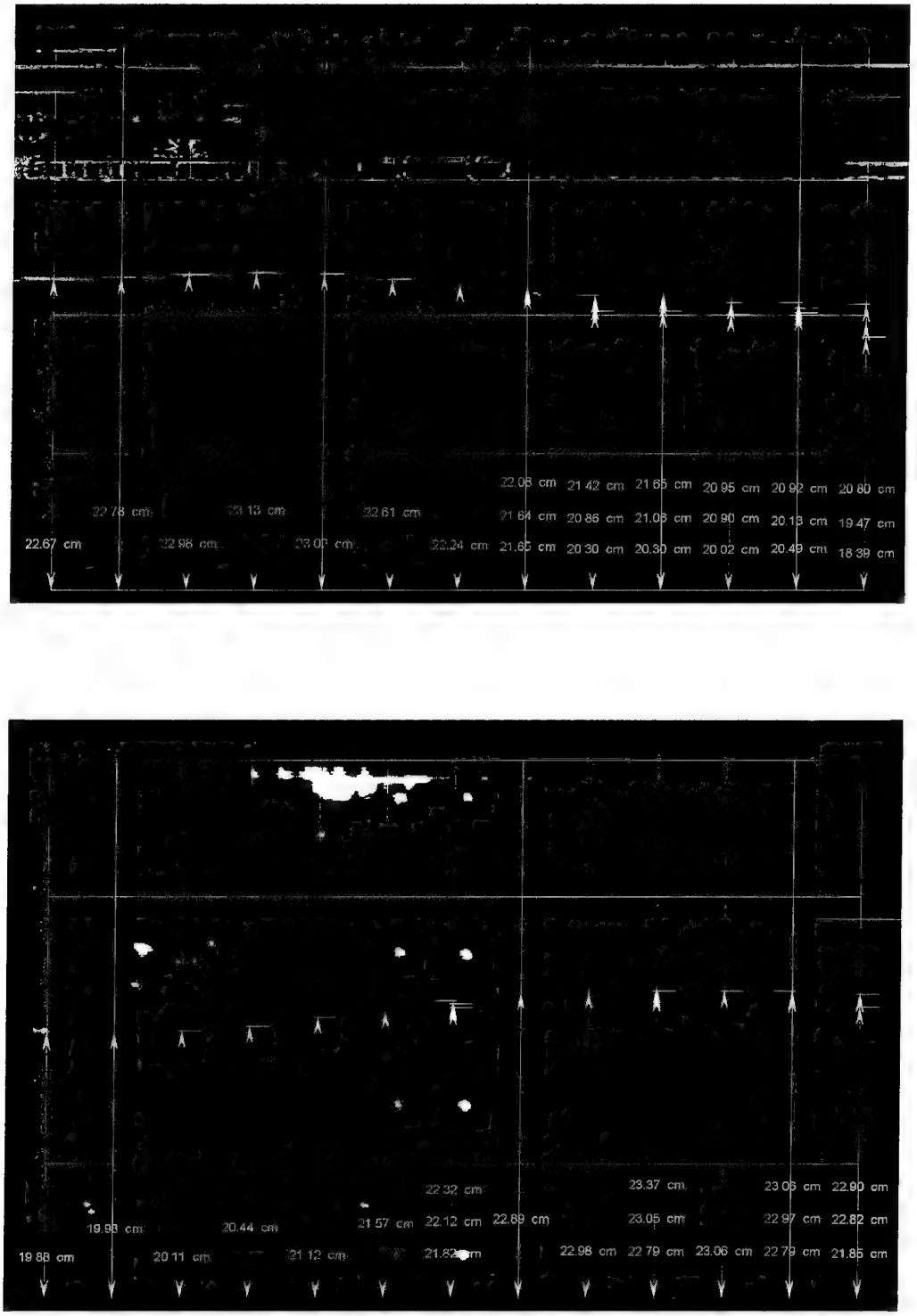

Figure 7. Typical images of cores of perturbed vortices: (a) side view; (b) plan view.

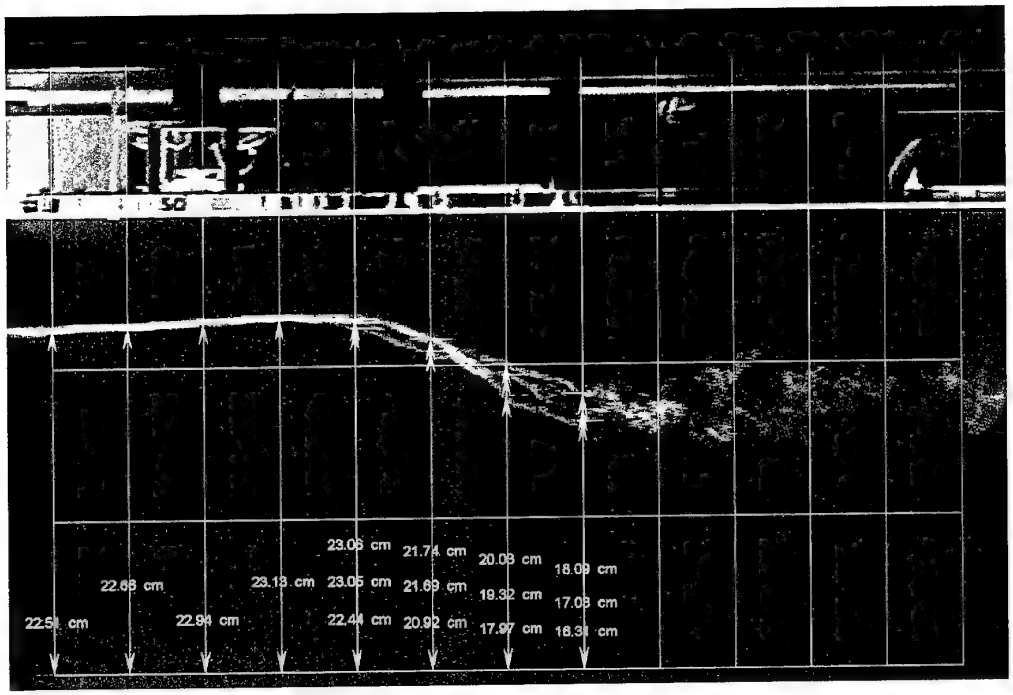

Figure 8. Typical images of cores of perturbed vortices that are partially destroyed: (a) side view; (b) plan view.

4. Analysis of Jet/Vortex Measurements

In this section, the jet/vortex measurements are analysed to determine the effects on the vortices of jet shape, jet velocity, jet location and jet pitch angle. An attempt is made to describe the interactions in terms of the physics of the flow processes.

4.1 Plots of Vortex Lateral Displacements

Side-view and plan-view images of cores of vortices were obtained for 42 different jet/vortex cases and the images were analysed using the technique described in Section 3.6 to determine core displacements, Δ_V and Δ_H, in the z_T and y_T directions respectively for different values of x_T. The complete set of experimental results is shown in Figure 9. In this figure, positive values of Δ_V denote core displacements away from the ground board and positive values of Δ_H denote core displacements towards port. The cases where a plotted trajectory stops before $x_T = 500$ mm indicates that the core of the vortex has been destroyed by the jet just after the last plotted point.

The plotted symbols and corresponding lines joining the symbols have been chosen to facilitate the interpretation of the experimental results. Data for circular jets are represented by a circle, namely ○, and data for rectangular jets are represented by a rectangle, namely ▭, ◇, ▯ or ◇, so that the orientation of the rectangle depicts the roll angle of the jet. For symbol ▭, corresponding to $\phi = 0°$, the long sides of the rectangular jet at its outlet are parallel to the tunnel free-stream velocity, and for symbol ▯, corresponding to $\phi = 90°$, the short sides of the rectangular jet are normal to the free-stream velocity. For symbol ◇, corresponding to $\phi = 45°$, the upstream long side of the rectangular jet is on the right-hand side when looking in the direction of the tunnel free-stream velocity, and conversely for symbol ◇, corresponding to $\phi = 135°$. Symbols for different jet velocities have different amounts of filling, so that data for $U_J = 0.4$ m/s are represented by an unfilled symbol, namely ○, ▭, ◇, ▯ or ◇, data for $U_J = 0.8$ m/s are represented by a partially filled symbol, namely ◉, ▬, ◈, ▮ or ◈, and data for $U_J = 1.2$ m/s are represented by a totally filled symbol, namely ●, ▬, ◆, ▮ or ◆. Symbols for jets located on the port side of the vortex, i.e. pro-vortex jets, are connected by full lines (——) and symbols for jets located on the starboard side of the vortex i.e. contra-vortex jets, are connected by broken lines (- - - -). Symbols for jets having different pitch angles (only applicable to the circular jets) incorporate a diagonal line that depicts the pitch angle of the jet, namely ∅, ◎ or ● for $\theta = -135°$, jet velocity inclined upstream, and ⊘, ◉ or ● for $\theta = -45°$, jet velocity inclined downstream. Symbols for vertical jets, i.e. $\theta = -90°$, do not incorporate a vertical line. The symbols and the lines connecting the symbols for the different types of jets are summarised in Table 1.

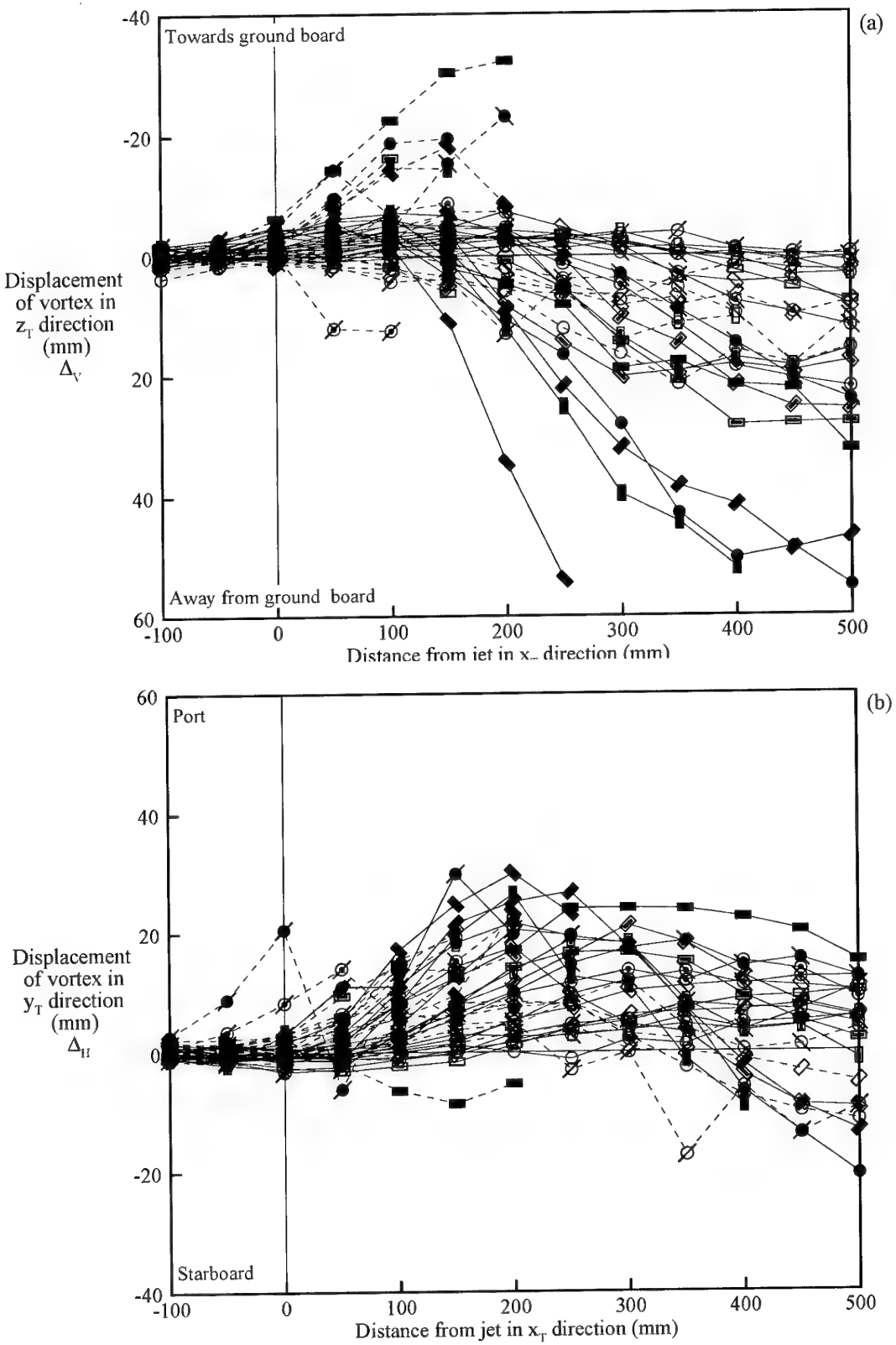

Figure 9. Effect of different jets on vortex displacement: (a) side view; (b) plan view. See Table 1 for an explanation of the symbols used for the different jets.

Table 1. Symbols and lines connecting the symbols for the different types of jets.

Symbol	Line connecting symbols	Jet velocity U_J (m/s)	Roll angle ϕ (degrees)	Pitch angle θ (degrees)	Yaw angle ψ (degrees)	Jet location y_T (mm)
○	———	0.4		–90	0	50 (pvj*)
◉	———	0.8		–90	0	50 (pvj)
●	———	1.2		–90	0	50 (pvj)
▭	———	0.4	0	–90	0	50 (pvj)
▣	———	0.8	0	–90	0	50 (pvj)
■	———	1.2	0	–90	0	50 (pvj)
◇	———	0.4	45	–90	0	50 (pvj)
◈	———	0.8	45	–90	0	50 (pvj)
◆	———	1.2	45	–90	0	50 (pvj)
▯	———	0.4	90	–90	0	50 (pvj)
▮	———	0.8	90	–90	0	50 (pvj)
▮	———	1.2	90	–90	0	50 (pvj)
◇	———	0.4	135	–90	0	50 (pvj)
◈	———	0.8	135	–90	0	50 (pvj)
◆	———	1.2	135	–90	0	50 (pvj)
⊘	———	0.4		–135	0	50 (pvj)
◉	———	0.8		–135	0	50 (pvj)
●	———	1.2		–135	0	50 (pvj)
⊘	———	0.4		–45	0	50 (pvj)
◉	———	0.8		–45	0	50 (pvj)
●	———	1.2		–45	0	50 (pvj)
○	-----	0.4		–90	0	–50 (cvj*)
◉	-----	0.8		–90	0	–50 (cvj)
●	-----	1.2		–90	0	–50 (cvj)
▭	-----	0.4	0	–90	0	–50 (cvj)
▣	-----	0.8	0	–90	0	–50 (cvj)
■	-----	1.2	0	–90	0	–50 (cvj)
◇	-----	0.4	45	–90	0	–50 (cvj)
◈	-----	0.8	45	–90	0	–50 (cvj)
◆	-----	1.2	45	–90	0	–50 (cvj)
▯	-----	0.4	90	–90	0	–50 (cvj)
▮	-----	0.8	90	–90	0	–50 (cvj)
▮	-----	1.2	90	–90	0	–50 (cvj)
◇	-----	0.4	135	–90	0	–50 (cvj)
◈	-----	0.8	135	–90	0	–50 (cvj)
◆	-----	1.2	135	–90	0	–50 (cvj)
⊘	-----	0.4		–135	0	–50 (cvj)
◉	-----	0.8		–135	0	–50 (cvj)
●	-----	1.2		–135	0	–50 (cvj)
⊘	-----	0.4		–45	0	–50 (cvj)
◉	-----	0.8		–45	0	–50 (cvj)
●	-----	1.2		–45	0	–50 (cvj)

* pvj = pro-vortex jet; cvj = contra-vortex jet

4.2 Theoretical Behaviour of Longitudinal Vortices

As a precursor to explaining vortex lateral movement, it is instructive to outline some classical background theory for free potential vortices in an ideal fluid –see for example Hunsaker & Rightmire (1947). For a single vortex, the induced circumferential velocity, U_I, at any point in the flow is given by $U_I = \Gamma/(2\pi r)$, where Γ is the strength or circulation of the vortex and r is the distance from the centre of the core of the vortex to the point under consideration, as depicted diagrammatically in Figure 10 (a). For a pair of vortices having equal strengths but opposite directions of rotation, as shown in Figure 10 (b), the induced velocities at the cores of the vortices are equal and the cores advance in the directions of the induced velocities as shown. For a pair of vortices having equal strengths and the same direction of rotation, as shown in Figure 10 (c), the induced velocities at the cores of the vortices cause the cores to rotate around a common centre as shown. It is assumed that this idealised theory can be used as a basis to explain why vortices move laterally in given directions in the current jet/vortex experiments. It is not expected that the theory will give precise details of the directions of vortex lateral displacements, but instead the theory will be used to give an indication of overall general trends in vortex behaviour.

4.3 Possible Explanations for Lateral Movement of Vortices

Figure 9 shows that when a vortex is subjected to jet flows the resulting behaviour of the core of the vortex can vary markedly for the different types of jets used. The core displacements can be towards the ground board, away from the ground board, to port, or to starboard. For increasing values of x_T, cores often exhibit corkscrew-type behaviour whereby lateral core displacements in the vertical and horizontal directions increase, reach a peak, and then decrease, sometimes changing sign. Jet and vortex flow fields become inextricably intertwined and the flow in the interaction regions becomes highly complex, making it difficult to interpret flow behaviour in these regions. Possible physical explanations for the vortex lateral movements for different types of jets are given below. Due to the complexity of the flows, the physical explanations are to some extent conjectural.

Rather than give physical explanations for vortex lateral movements for all of the jet/vortex cases shown in Figure 9, discussion will be restricted to six types of jets, comprising pro-vortex and contra-vortex circular jets (see Section 3.4) having velocities of 0.4, 0.8 and 1.2 m/s in a direction 90° (initially) to the direction of the cross-flow. Experiments on circular jets whose velocity is normal to the cross-flow are the most widely reported in the literature. Plots of vortex lateral displacements corresponding to the six selected jet/vortex cases are shown in Figure 11. The data in this figure were obtained from Figure 9. Flow-visualization images for the six selected cases are shown in Figures 12 to 17. The two dye circuits on the vortex apparatus (Section 3.2.1) and the single dye circuit on the jet apparatus (Section 3.2.2) were used to enable the cores and the outer-flow regions of the vortices and the outer-flow regions of the jets to be

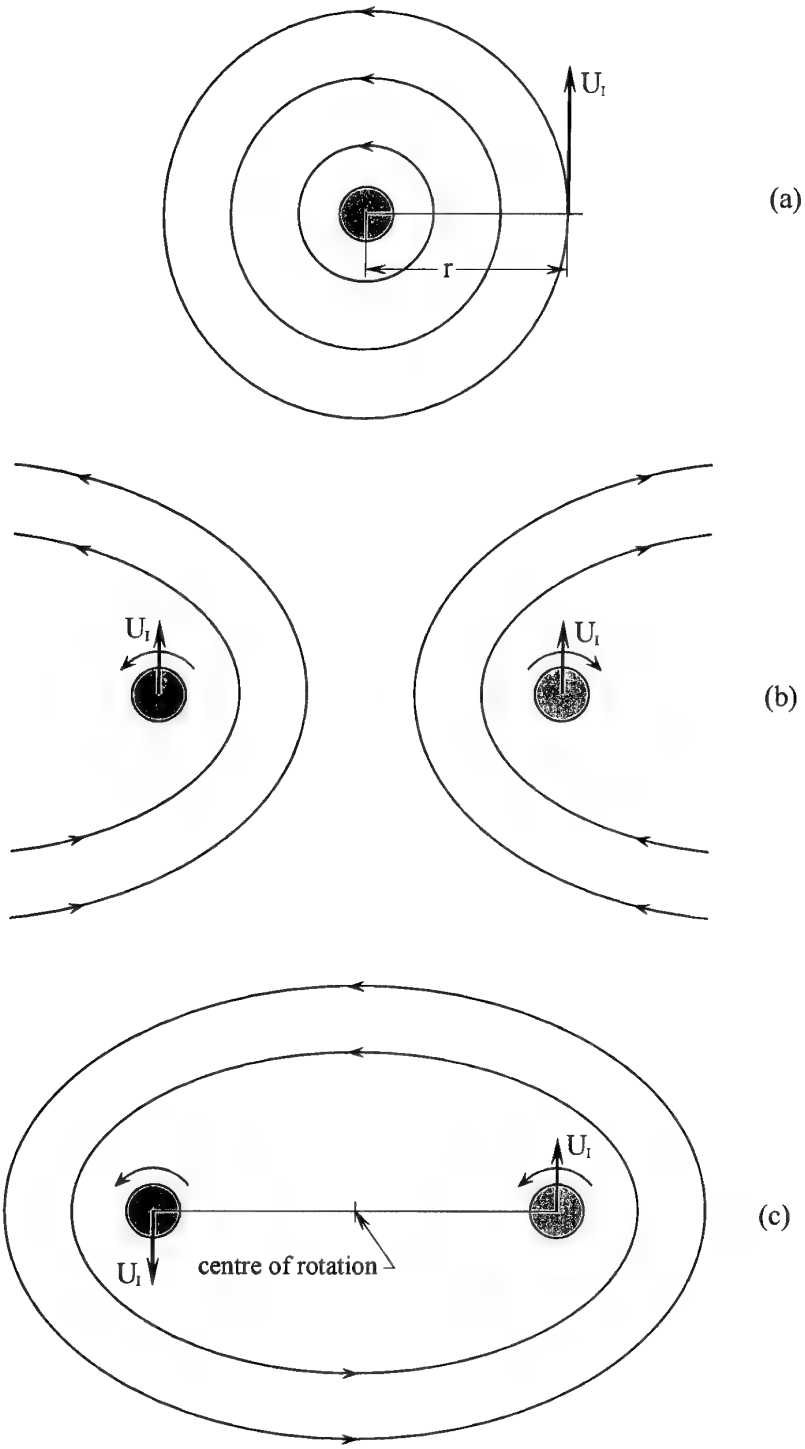

Figure 10. Idealised vortices showing streamlines and induced velocities: (a) single potential vortex; (b) vortex pair with opposite directions of rotation; (c) vortex pair with the same direction of rotation (based on a diagram given by Hunsaker & Rightmire 1947).

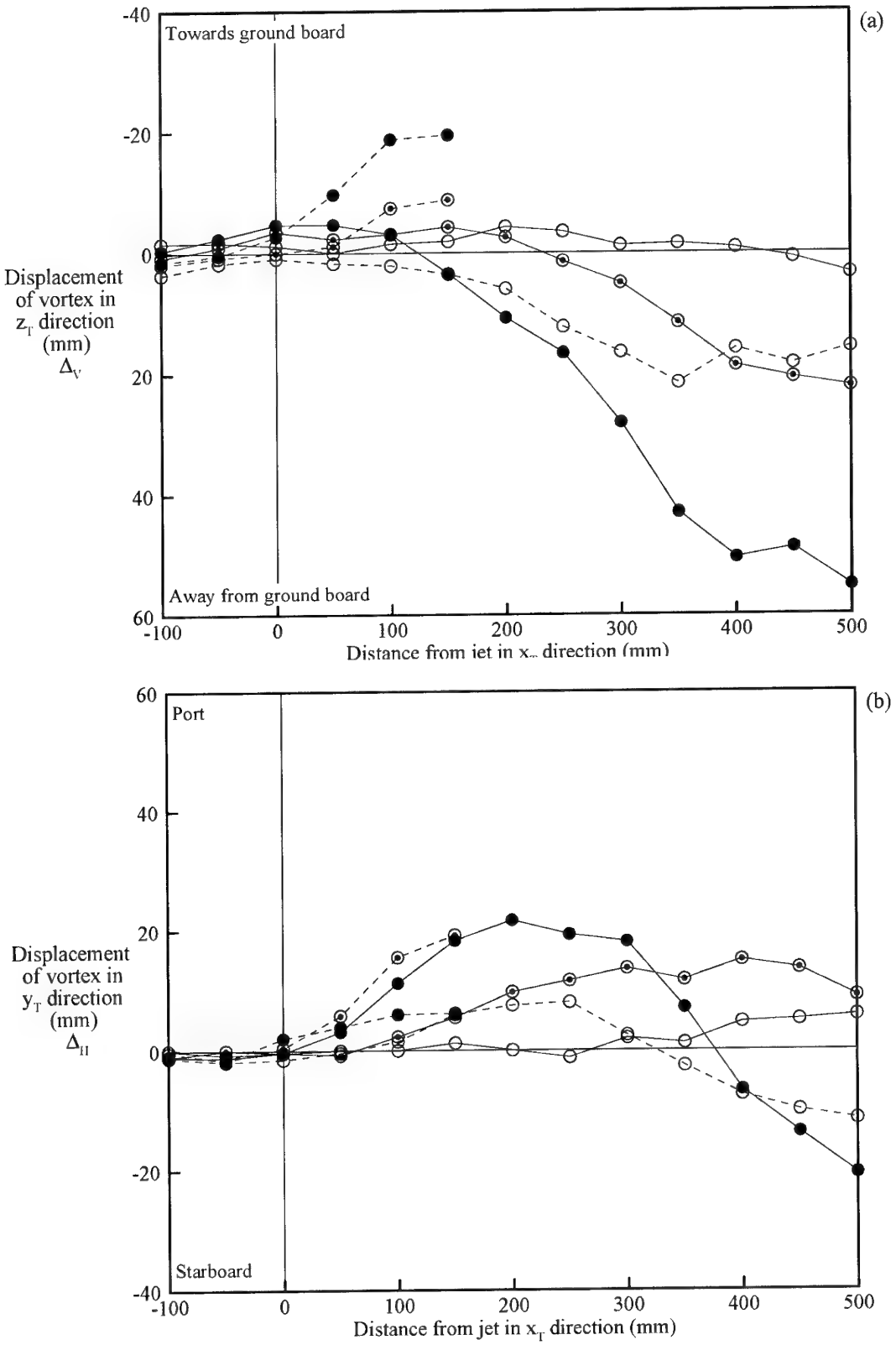

Figure 11. Effect of different jets on vortex displacement: (a) side view; (b) plan view. See Table 1 for an explanation of the symbols used for the different jets.

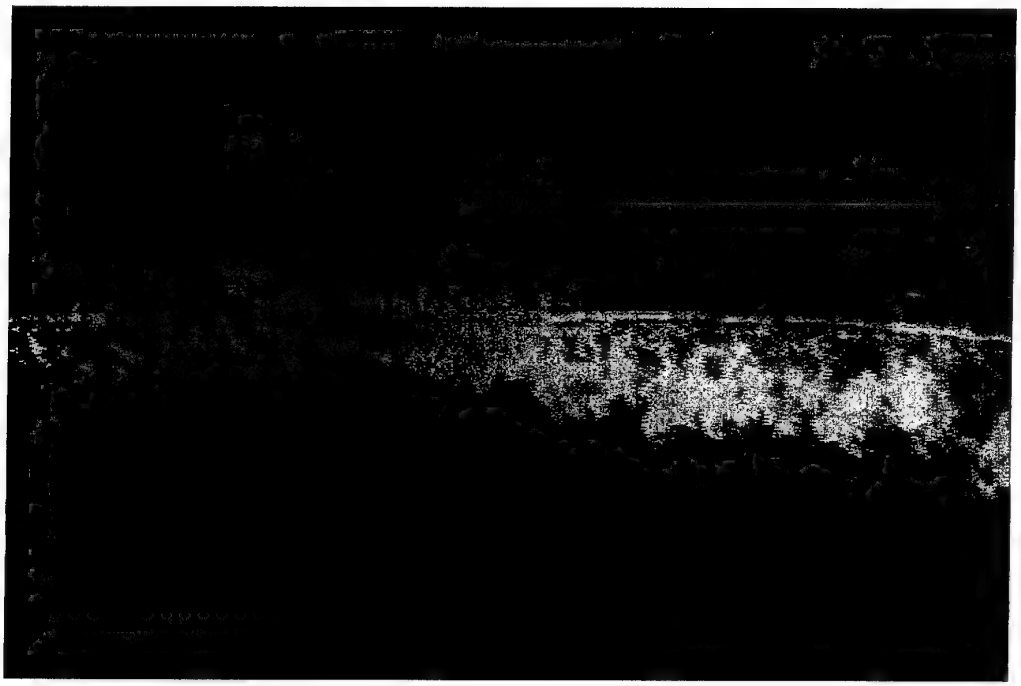

(a)

(b)

Figure 12. Flow-visualization images of a jet/vortex interaction. Circular jet, $U_j = 0.4$ m/s, pro-vortex jet, $\theta = -90°$: (a) side view; (b) plan view.

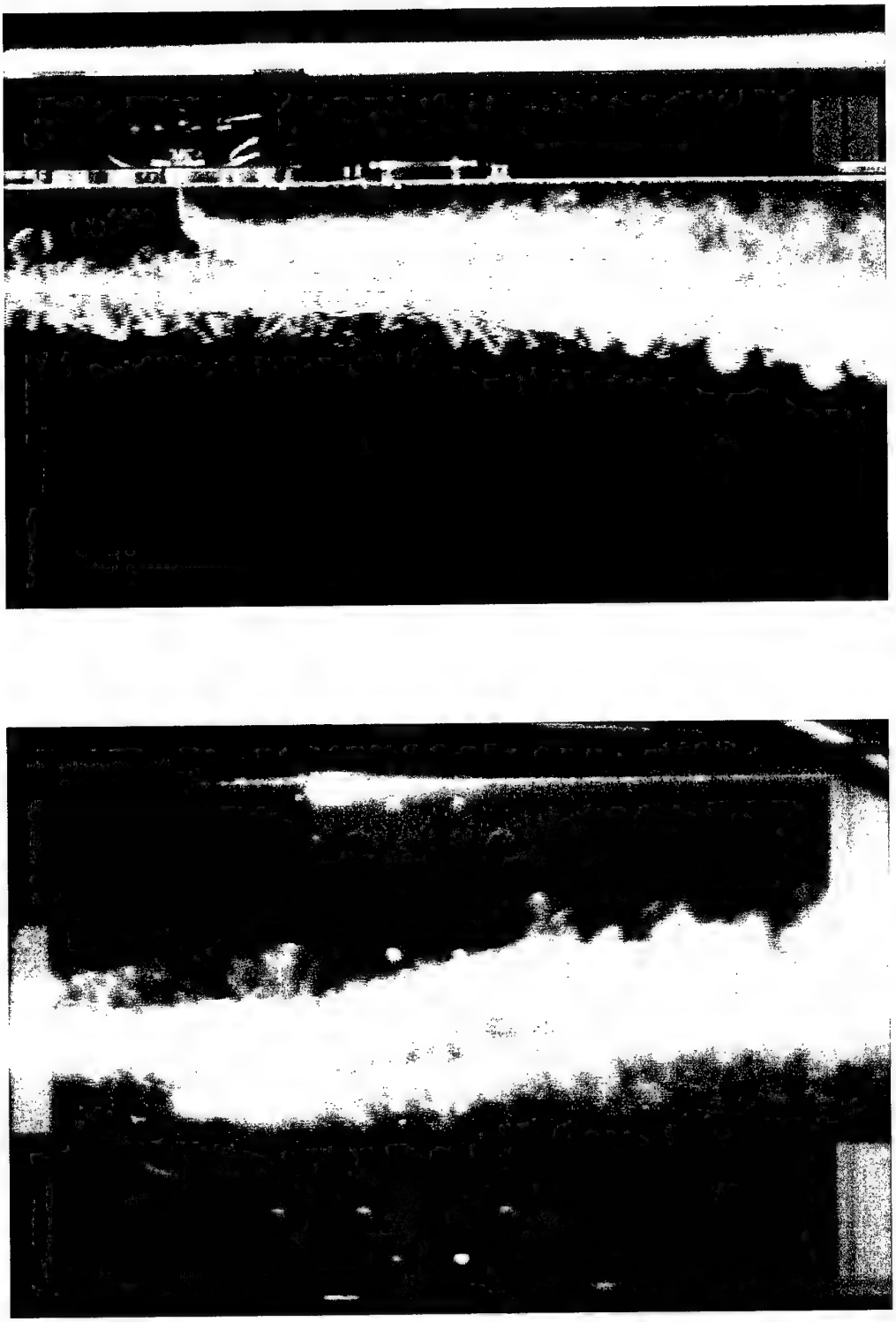

Figure 13. Flow-visualization images of a jet/vortex interaction. Circular jet, U_j = 0.4 m/s, contra-vortex jet, θ = –90°: (a) side view; (b) plan view.

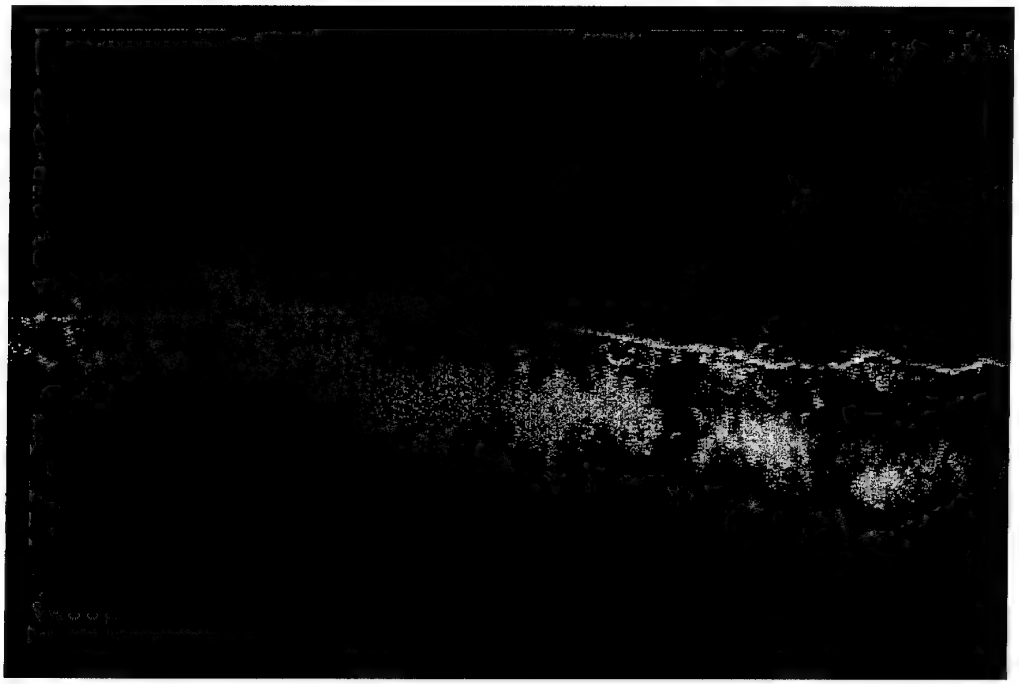

(a)

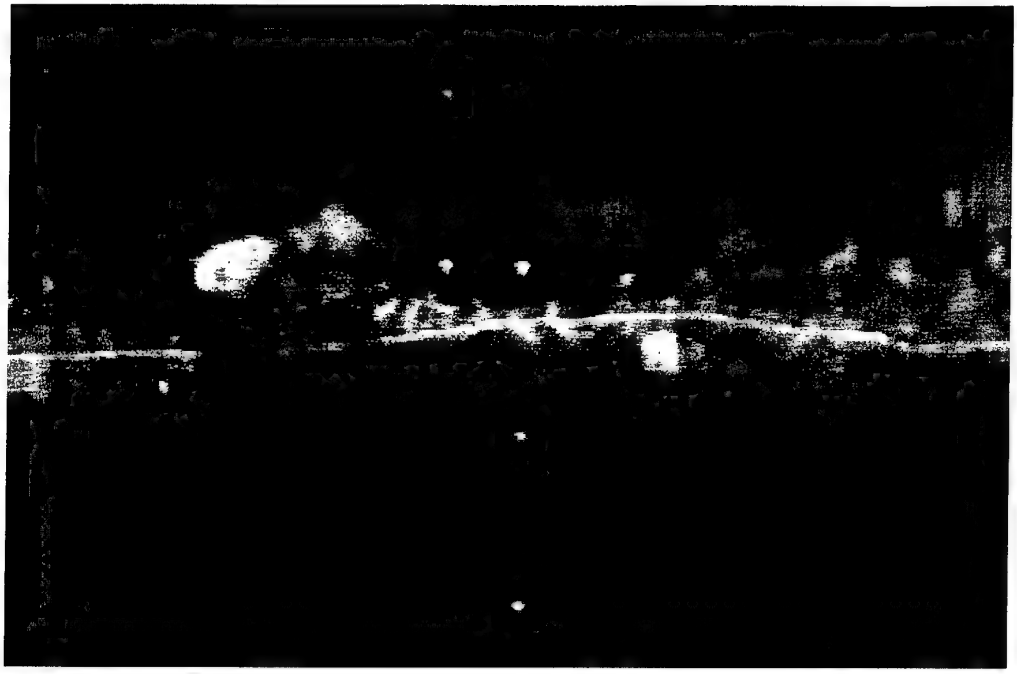

(b)

Figure 14. Flow-visualization images of a jet/vortex interaction. Circular jet, $U_J = 0.8$ m/s, pro-vortex jet, $\theta = -90°$: (a) side view; (b) plan view.

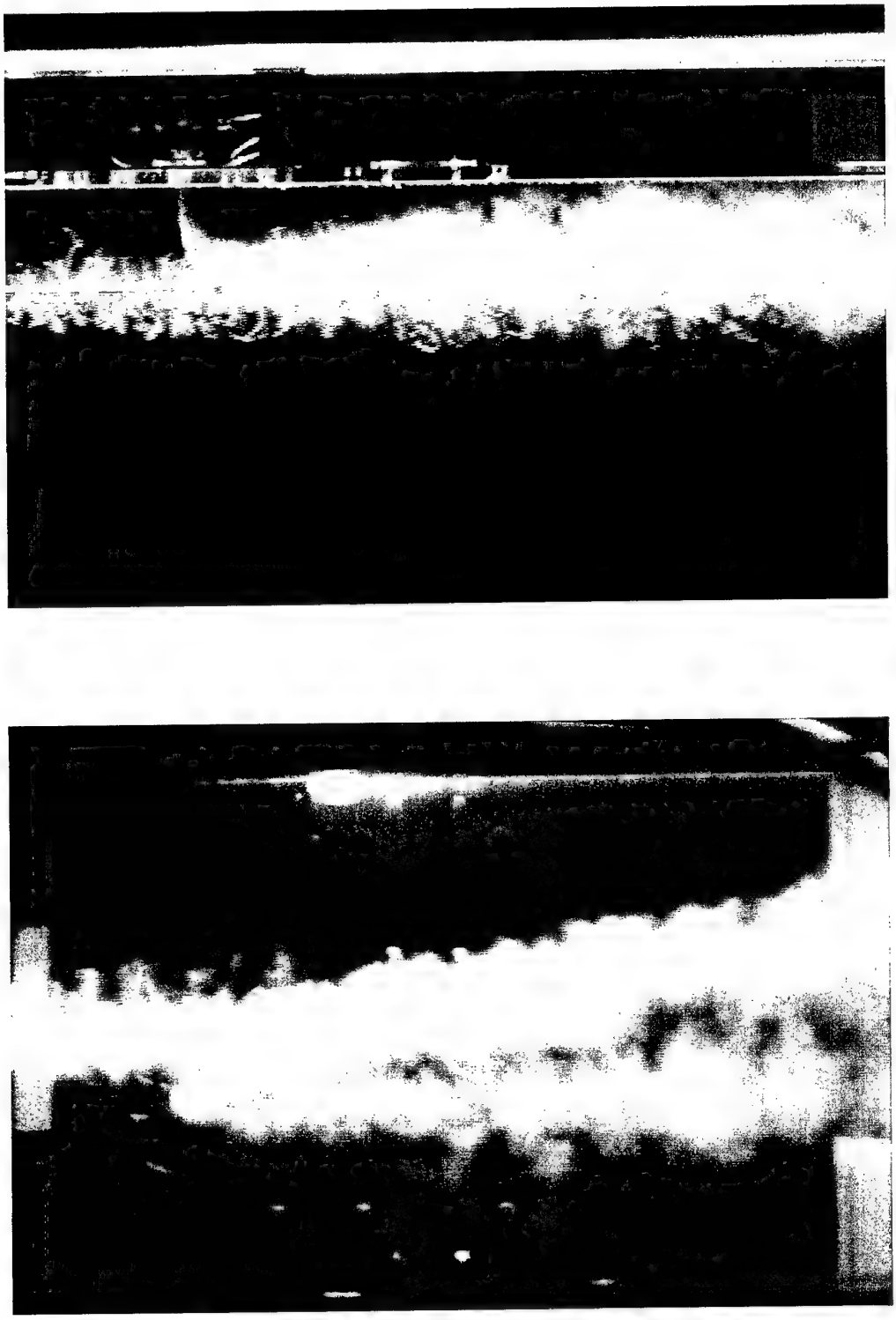

Figure 15. Flow-visualization images of a jet/vortex interaction. Circular jet, U_j = 0.8 m/s, contra-vortex jet, θ = –90°: (a) side view; (b) plan view.

(a)

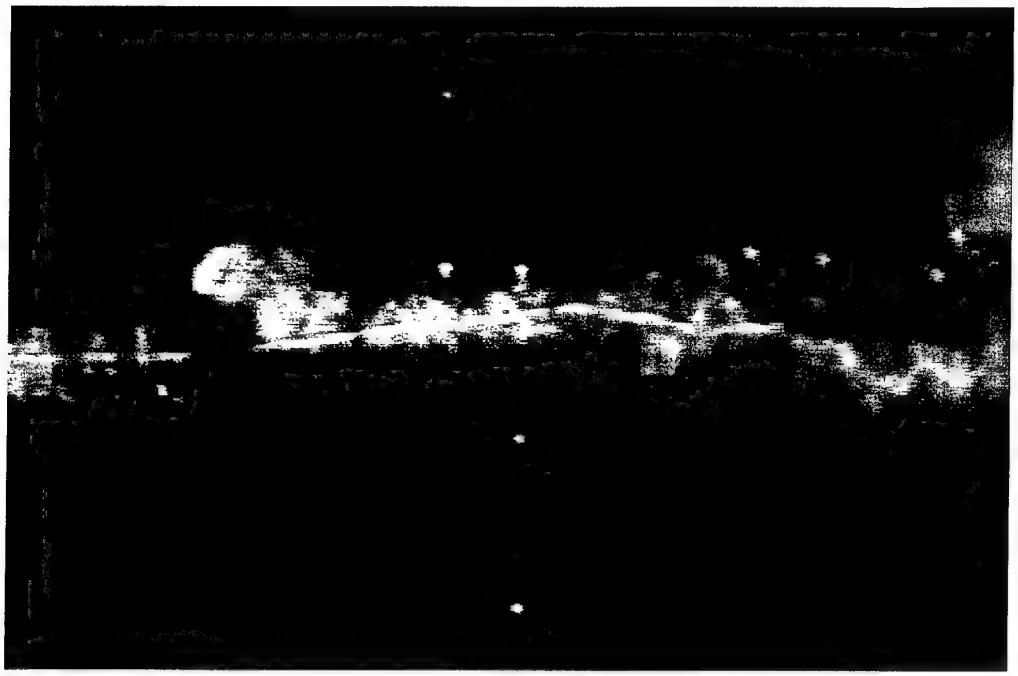

(b)

Figure 16. Flow-visualization images of a jet/vortex interaction. Circular jet, U_j = 1.2 m/s, pro-vortex jet, θ = –90°: (a) side view; (b) plan view.

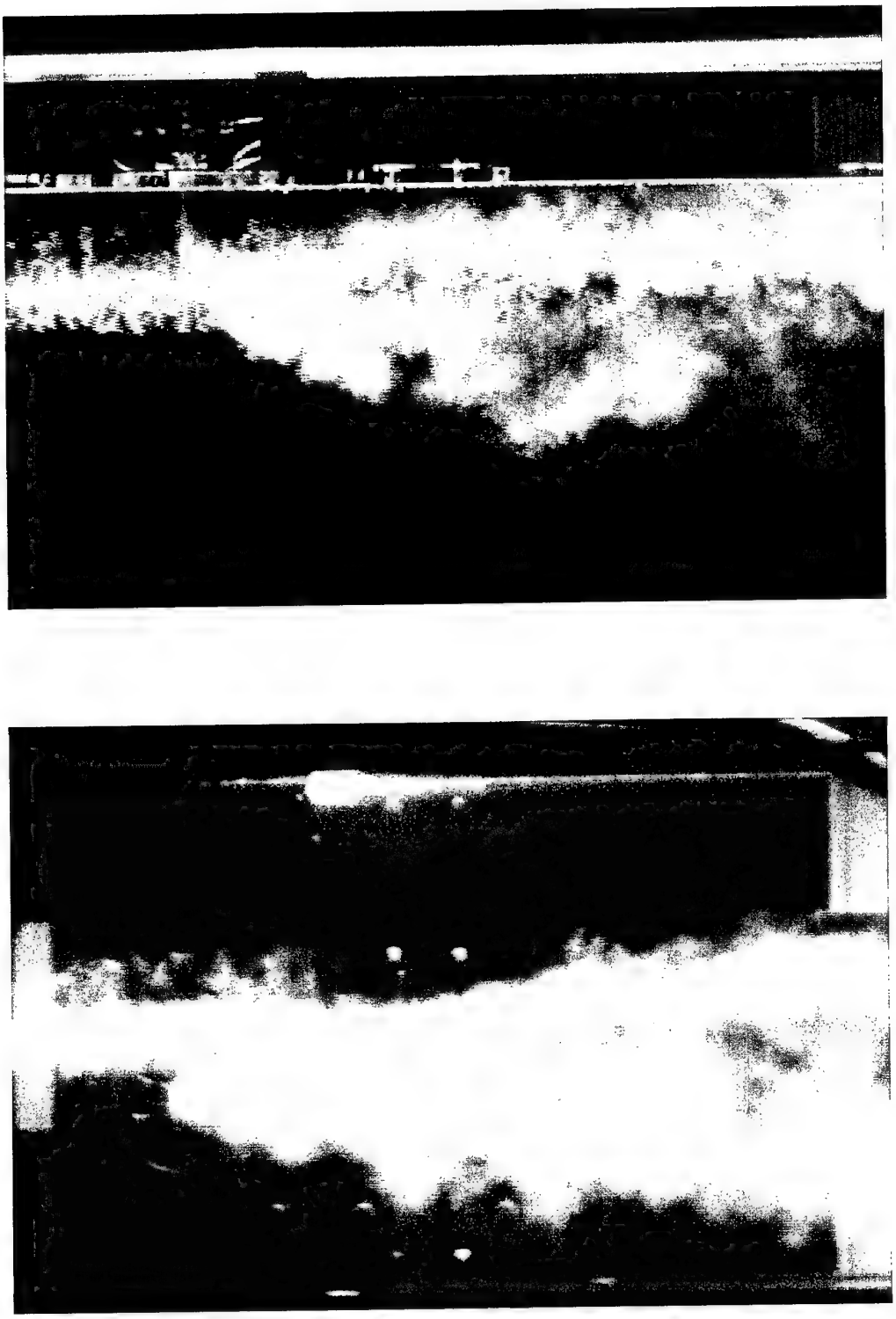

Figure 17. Flow-visualization images of a jet/vortex interaction. Circular jet, U_j = 1.2 m/s, contra-vortex jet, θ = –90°: (a) side view; (b) plan view.

visualized. The jet/vortex images in Figures 12 to 17 indicate the relative strengths of the vortices and the jets. Clearly the vortices and jets are well matched, in terms of strength, since a "weak" jet would be wrapped around a "strong" vortex and vice versa.

Figures 18 to 23 depict idealised vortex and jet cross sections in the y_T z_T transverse plane (see Figure 2) for $x_T \approx 100$ and 300 mm ($x_T/D \approx 15$ and 45 respectively), corresponding to the jet/vortex images shown in Figures 12 to 17 respectively. In Figures 18 to 23, the direction of the tunnel free-stream velocity is out of the page. The above x_T distances are far enough downstream from the jet outlet for the mean directions of the jet flows to be predominantly in the direction of the tunnel free-stream. For purposes of explaining directions of vortex lateral movements, the jets in Figures 18 to 23 have been drawn with a uniform shape and size, and likewise for the vortices, even though the shapes and sizes of the jets and vortices can vary depending on the particular jet/vortex interaction and value of x_T considered. No allowance has been made for deformation of the jets and vortices resulting from the mixing of the jet and vortex flows.

The two symmetrical counter-rotating vortices forming the jets both induce velocities at the core of the main vortex emanating from the aerofoil, causing this vortex to move laterally. The effect that each of these jet vortices has on the main vortex for the different cases depends on the position of the jet relative to the main vortex. On Figures 18 to 23, suggested directions of the induced velocities at the core of the main vortex, resulting from interaction with each of the two jet vortices, are indicated by arrowed lines through the core of the main vortex (thin lines with small arrowheads). Such lines are drawn perpendicular to the lines connecting the core of the main vortex and the cores of the jet vortices under consideration. The directions and lengths of these arrowed lines are based on the idealised theory outlined above. The length of each arrowed line has been drawn to be proportional to the magnitude of the induced velocity, and the lengths are based on the distance between the core of a main vortex and the core of a jet vortex. The resultant direction of the induced velocity at the core of the main vortex is also indicated by an arrowed line (thick lines with large arrowheads). Note that the arrowed lines in Figures 18 to 23 denote directions of induced velocities, and hence directions of vortex movement, and not magnitudes of vortex displacements. This means, for example, that the main vortex may be displaced towards port, relative to its unperturbed state, but be moving towards starboard (as shown in Figure 11 (b) at $x_T \approx 300$ mm ($x_T/D \approx 45$) for the case of the pro-vortex circular jet having $U_J = 1.2$ m/s). Suggested directions of movement of the counter-rotating jet vortices, resulting from interaction with each other and with the main vortex, are not indicated by arrows since lateral movements of the jets are not the prime concern in the current investigation.

It is encouraging that the suggested resultant directions of movement of the core of the main vortex for the different cases, shown in Figures 18 to 23, show agreement with the measured directions of the movement indicated in Figure 11, and this gives some credibility to the method of analysis. The higher the jet velocity the greater the strength of the jet vortices and the induced velocities (according to the idealised theory), and consequently the greater the rate of deflection and the deflection of the main vortex.

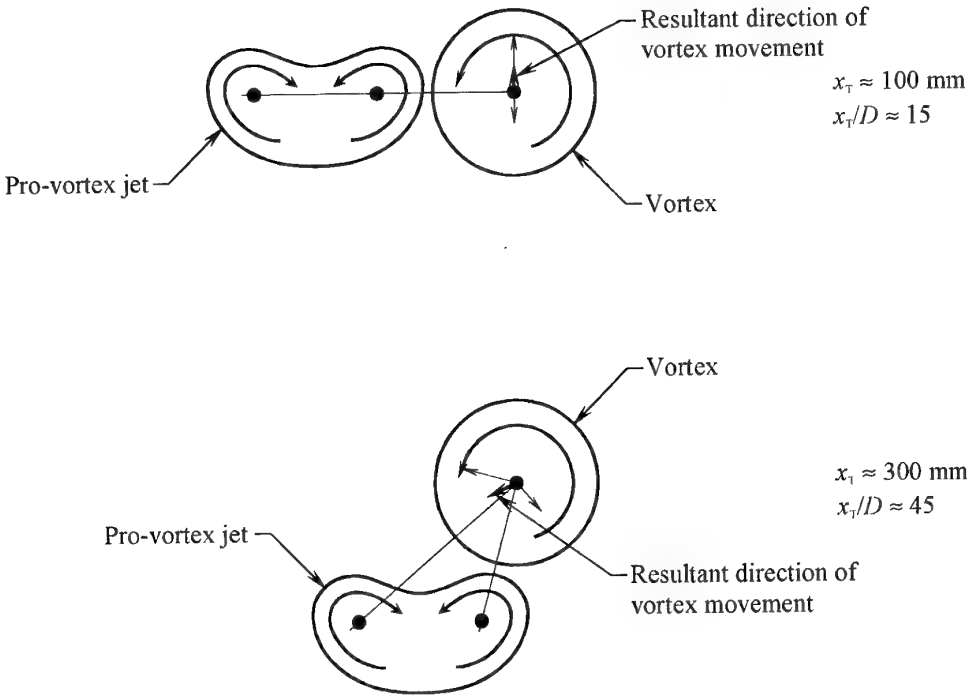

Figure 18. Cross sections of a vortex and a jet showing the direction of vortex movement. Circular jet, $U_J = 0.4$ m/s, pro-vortex jet, $\theta = -90°$.

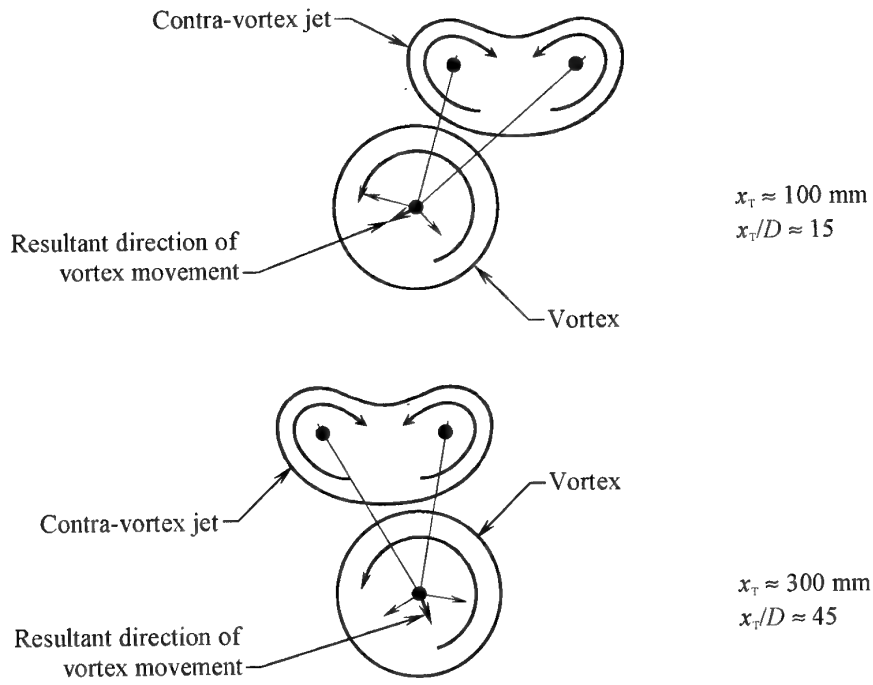

Figure 19. Cross sections of a vortex and a jet showing the direction of vortex movement. Circular jet, $U_J = 0.4$ m/s, contra-vortex jet, $\theta = -90°$.

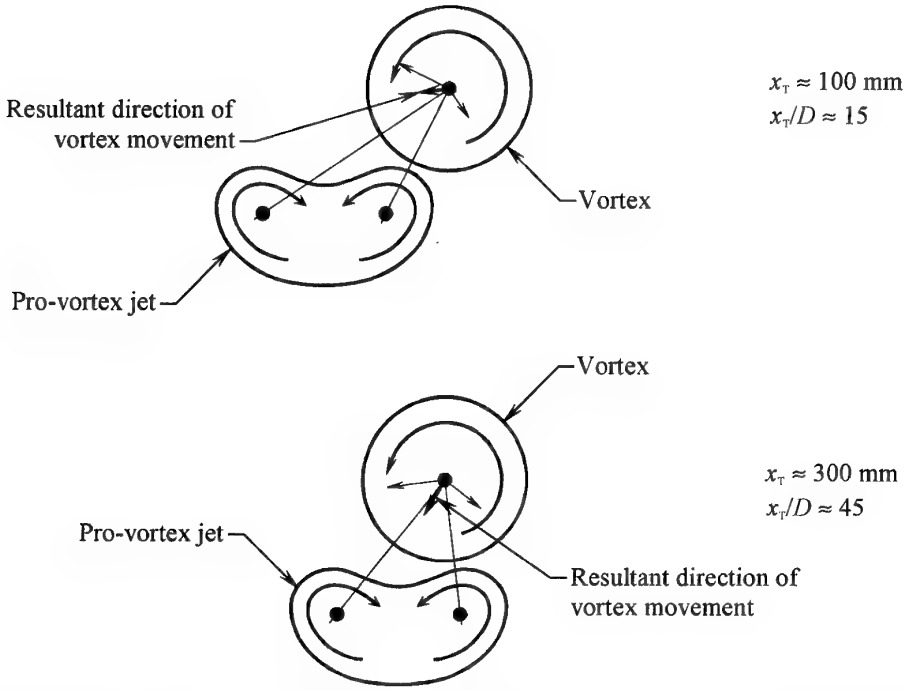

Figure 20. Cross sections of a vortex and a jet showing the direction of vortex movement. Circular jet, $U_J = 0.8$ m/s, pro-vortex jet, $\theta = -90°$.

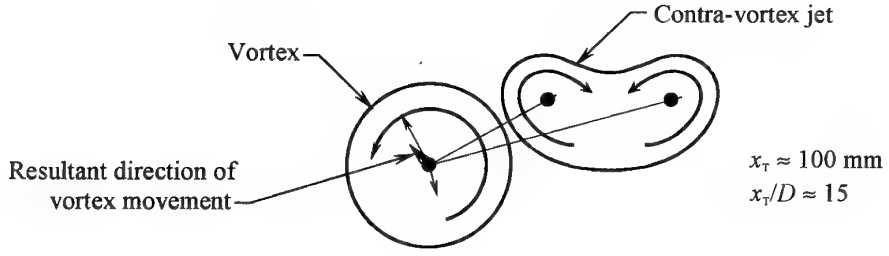

Figure 21. Cross sections of a vortex and a jet showing the direction of vortex movement. Circular jet, $U_J = 0.8$ m/s, contra-vortex jet, $\theta = -90°$.

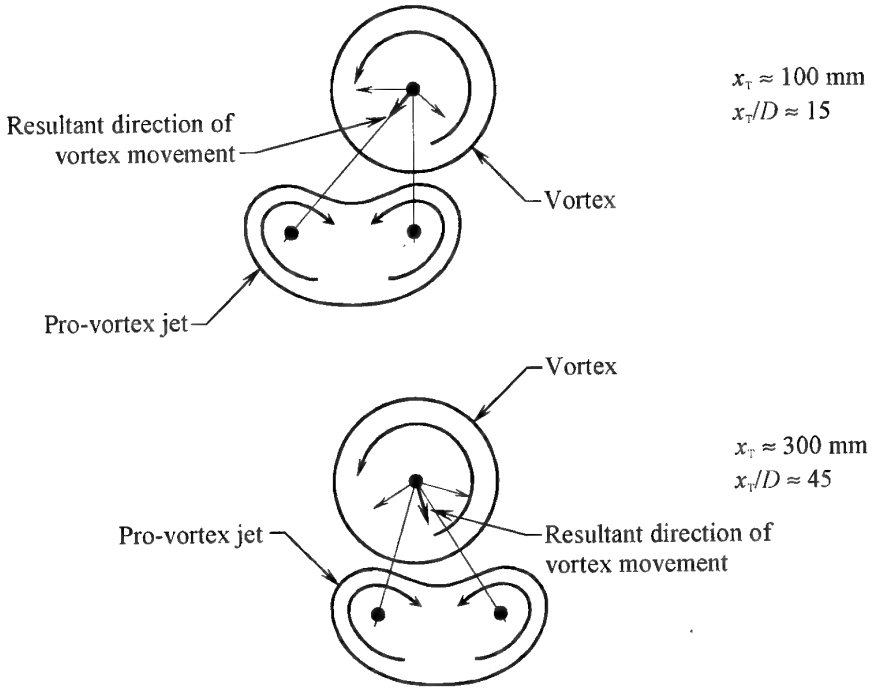

Figure 22. Cross sections of a vortex and a jet showing the direction of vortex movement. Circular jet, $U_J = 1.2$ m/s, pro-vortex jet, $\theta = -90°$.

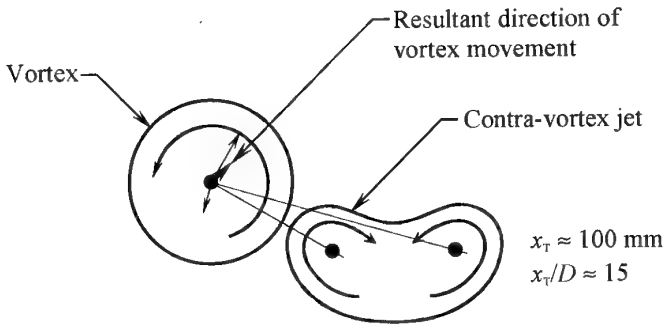

Figure 23. Cross sections of a vortex and a jet showing the direction of vortex movement. Circular jet, $U_J = 1.2$ m/s, contra-vortex jet, $\theta = -90°$.

Figure 11 shows that the rate of change of lateral displacements generally increases with increasing jet velocity, as expected. However, in Section 4.5.2 it is shown that increasing the jet velocity is only beneficial up to a certain point, beyond which further increase in jet velocity has no positive effect.

4.4 Replotting of Vortex Lateral Displacements

The effects on core displacements of the different jets are not easily discernible for the 42 different curves plotted in each of Figures 9 (a) and 9 (b). The interaction process is most likely non-linear so that the core displacement resulting from simultaneously varying two or more jet parameters will, in general, probably be different from the sum of the individual core displacements resulting from varying the parameters separately. In an attempt to isolate the effects of the different jet parameters, the data in Figure 9 have been replotted. The procedure used to do this will be described for the side-view data (Figure 9 a), but an identical procedure was used for the plan-view data (Figure 9 b). Data in Figure 9 (a) have been replotted in four different figures, namely Figures 24, 26, 28 and 30, to indicate the effects on core displacements of jet shape, jet velocity, jet location and jet pitch angle respectively. The data in each of these four figures have been plotted on a number of sets of axes –Figures 24, 26, 28 and 30 contain 6, 14, 21 and 6 sets of axes respectively. The data have been plotted in this way to isolate the effects of variation of a given jet parameter, i.e. only one parameter varies on each set of axes. For example, jet shape is the only variable in each of Figures 24 (a) to (f) (recalling that rectangular jets at different roll angles are classified as different jet shapes). Plan-view data, corresponding to the side-view data shown in Figures 24, 26, 28 and 30, are shown in Figures 25, 27, 29 and 31 respectively.

4.5 Effects of the Different Jet Parameters

4.5.1 Effects of Jet Shape

Five different jet shapes were used in the current investigation. A nozzle having a circular outlet and a nozzle having a rectangular outlet were used. The rectangular nozzle was set at roll angles, ϕ, of 0°, 45°, 90° and 135° (i.e. four jet shapes).

Figures 24 and 25 show that jet shape can have a significant effect on vortex displacement. For $U_J = 1.2$ m/s, values of Δ_V and Δ_H for the rectangular jet vary markedly depending on the roll angle of the nozzle, as shown in Figures 24 (c) and (f) and 25 (c) and (f).

To help explain the large differences in vortex displacements for the different jet configurations, it was necessary to carry out further flow-visualization experiments using different nozzles. The circular nozzle and the rectangular nozzle set at different roll angles were used. For these tests, the cambered plate used to generate the longitudinal vortex (see Figure 4) was not in the tunnel. Details of the different nozzle

configurations used and the corresponding observed transverse flow cross sections of the jets (looking upstream along the test section of the tunnel) are shown in Figure 32. The diagrams shown are only meant to convey the basic forms of the jet vortices and the directions of rotation, and not the strengths or sizes of the different jet vortices. It was found that when the jet flows were symmetrical with the cross flow, which occurred for the circular nozzle and for the rectangular nozzle set at roll angles of 0° and 90°, the jets were comprised of a pair of symmetrical counter-rotating vortices for jet velocities of 0.4, 0.8 and 1.2 m/s. However, for asymmetrical jet flows, which occurred when the rectangular nozzle was set at roll angles of 45° and 135°, the jets were comprised of a strong dominant vortex and a very weak counter-rotating vortex for the three velocities. When the rectangular nozzle was set at $\phi = 45°$, the dominant vortex rotated in an anti-clockwise direction when looking upstream, and conversely for the $\phi = 135°$ case.

The jet behaviour for rectangular nozzles set at $\phi = 45°$ and 135° is consistent with that found by Zhang & Collins (1997), who also tested rectangular jets. In their case the jet nozzle was pitched and yawed and the velocity ratios used were low (≤ 2.0) so that the jets remained within the wall boundary layer. They indicated that initially two vortices were formed, but the less dominant vortex was dissipated quickly. Similar results were obtained by Johnston & Nishi (1990) with pitched and yawed circular jets (velocity ratios ≤ 1.0). They reported that such jets were comprised of a single vortex and they gave no indication of whether there was initially a strong and a weak vortex. The foregoing suggests that jets are only comprised of symmetrical counter-rotating vortices if the jet flow is symmetrical with the cross flow.

The lateral spread of the jets was found to be different for the circular nozzle and for the rectangular nozzle set at different roll angles, due to the different transverse dimensions of the orifices of the different nozzles. In Section 2, it was indicated that the jet counter-rotating vortices were formed from the roll up of the vorticity at the sides of a nozzle orifice, and that the vortices at the leading and trailing edges of the orifice were considered to annul each other. Since the extent of the leading and trailing edges varies for the different nozzles, the foregoing suggests that the different nozzles may produce jet vortices of different strengths. For the rectangular jet set at $\phi = 0°$, the vortices were found to be more distinct and smaller than those for the rectangular jet set at $\phi = 90°$.

The large variations in vortical displacements for different jet shapes, shown in Figures 24 (c) and (f) and 25 (c) and (f), are most likely due to the fact that the controlling jet emerging from the rectangular nozzle drastically changed its shape as the nozzle was rolled, as explained above. However, the exact physical flow mechanisms for the different transverse displacements of the longitudinal vortex are unclear. It is not jet shape alone that causes the above large variations in transverse vortical behaviour, since in some cases, such as those shown in Figures 24 (a) and 25 (a), jet shape has little effect. It is the combination of several factors, such as jet shape, jet velocity and jet location, that cause the large variations. In Section 4.5.5, the jets that produce the largest vertical and the largest horizontal lateral displacements will be discussed.

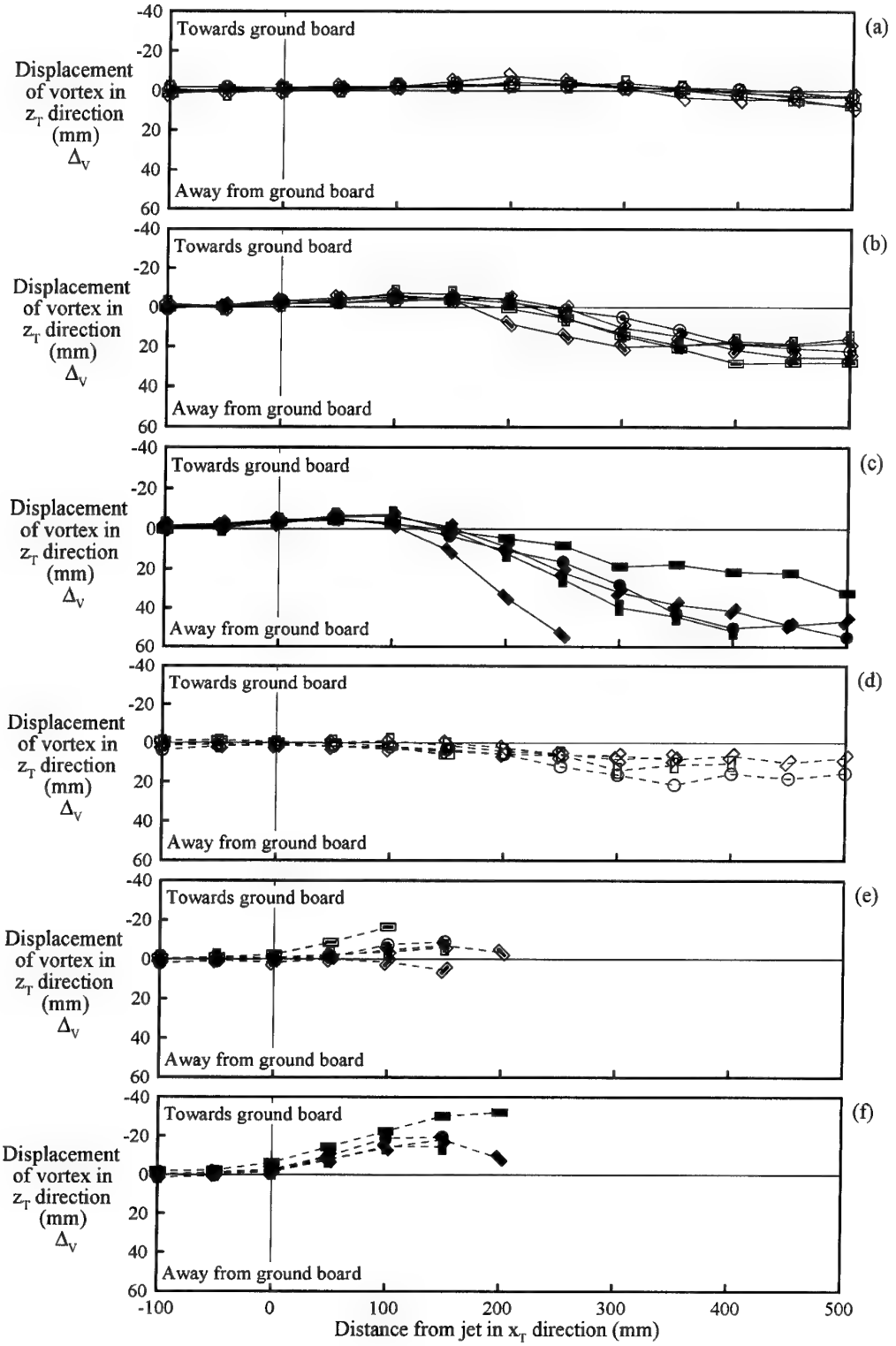

Figure 24. Effect of jet shape on vortex displacement –side views: (a) U_J = 0.4 m/s, pvj, θ = –90°; (b) U_J = 0.8 m/s, pvj, θ = –90°; (c) U_J = 1.2 m/s, pvj, θ = –90°; (d) U_J = 0.4 m/s, cvj, θ = –90°; (e) U_J = 0.8 m/s, cvj, θ = –90°; (f) U_J = 1.2 m/s, cvj, θ = –90°. See Table 1 for an explanation of the symbols used for the different jets.

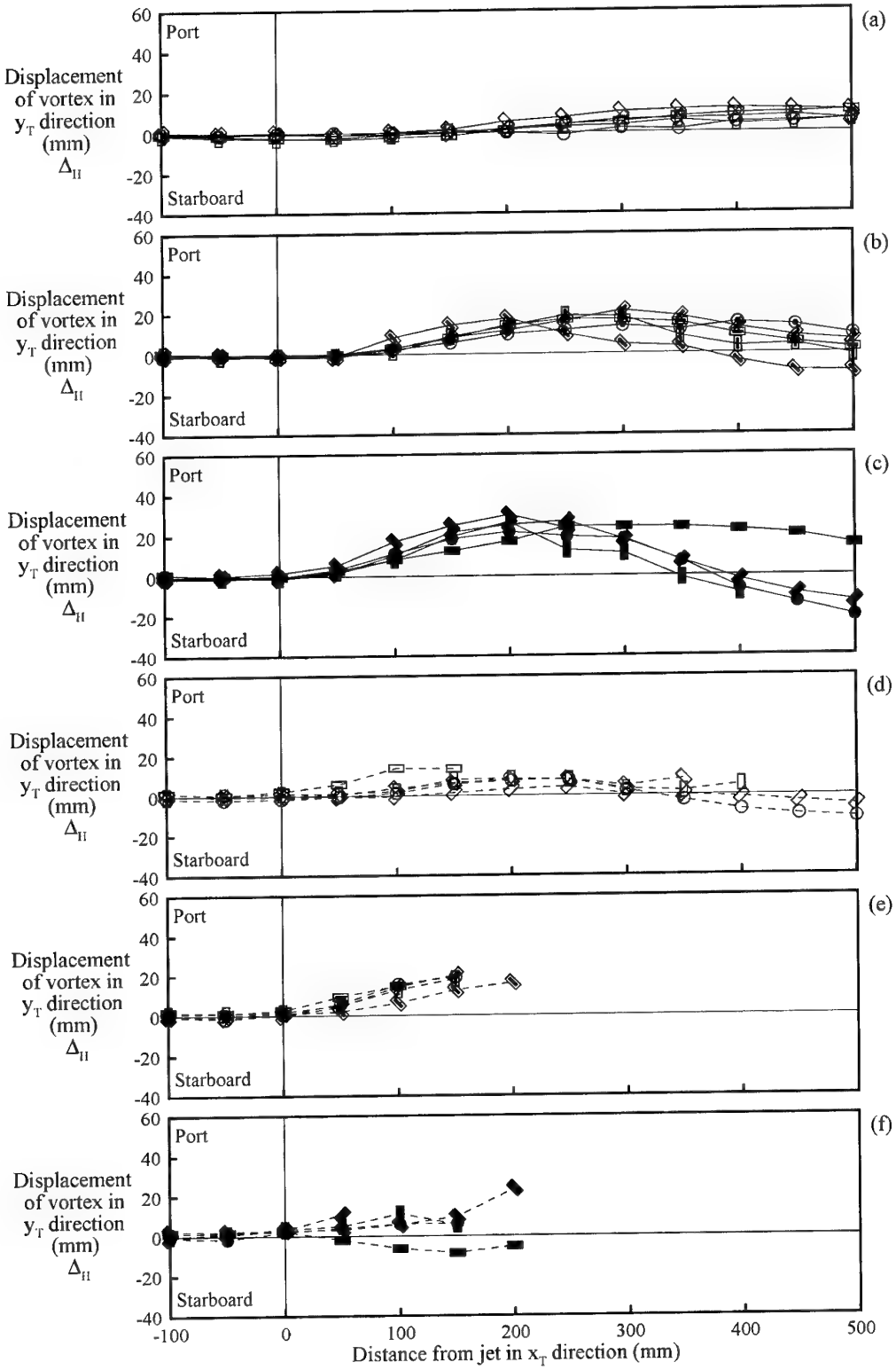

Figure 25. Effect of jet shape on vortex displacement plan views:
(a) U_J = 0.4 m/s, pvj, θ = -90°; (b) U_J = 0.8 m/s, pvj, θ = -90°; (c) U_J = 1.2 m/s, pvj, θ = -90°;
(d) U_J = 0.4 m/s, cvj, θ = -90°; (e) U_J = 0.8 m/s, cvj, θ = -90°; (f) U_J = 1.2 m/s, cvj, θ = -90°.
See Table 1 for an explanation of the symbols used for the different jets.

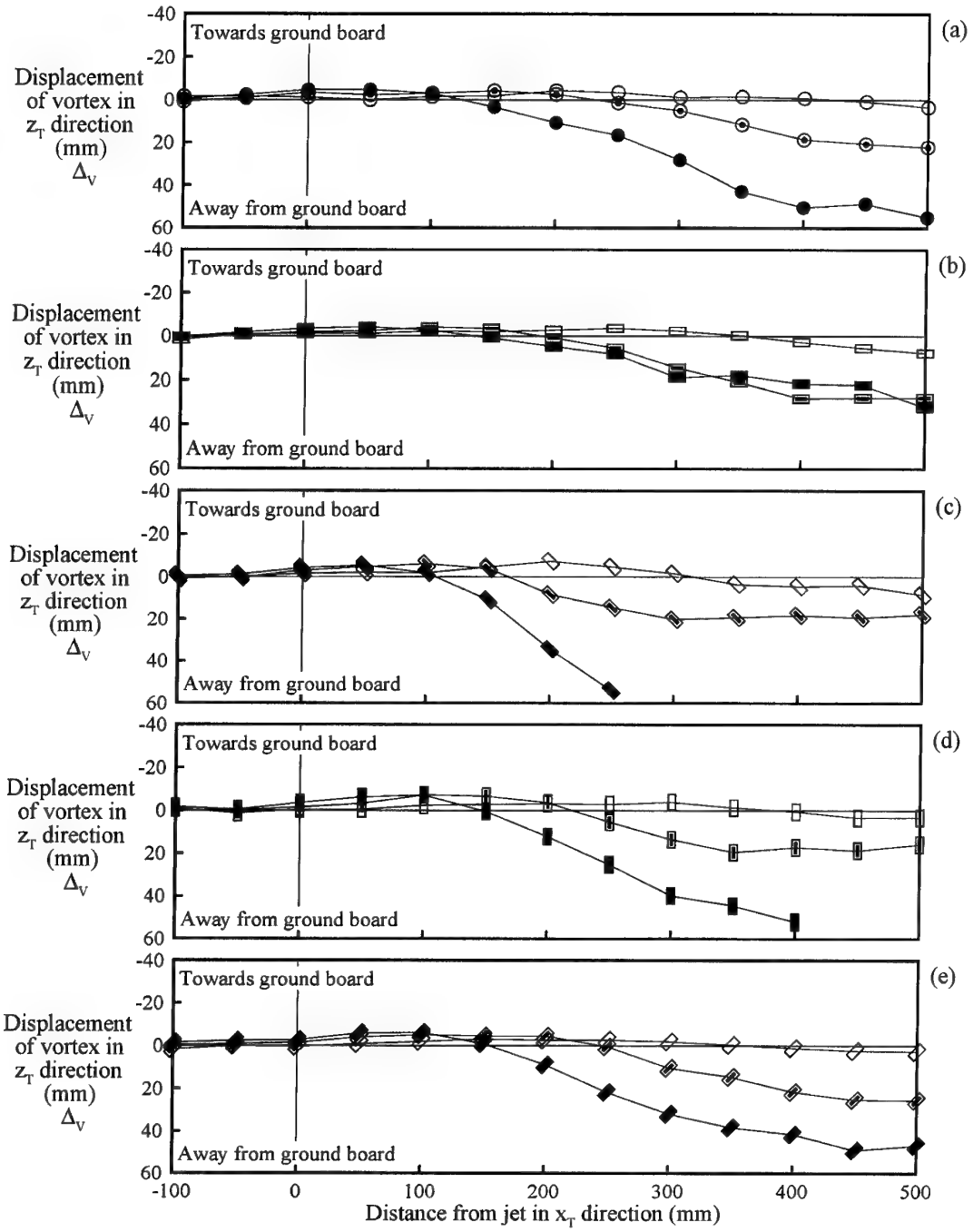

Figure 26. Effect of jet velocity on vortex displacement –side views: (a) circular jet, pvj, θ = –90°; (b) rectangular jet ϕ = 0°, pvj, θ = –90°; (c) rectangular jet ϕ = 45°, pvj, θ = –90°; (d) rectangular jet ϕ = 90°, pvj, θ = –90°; (e) rectangular jet ϕ = 135°, pvj, θ = –90°. See Table 1 for an explanation of the symbols used for the different jets.

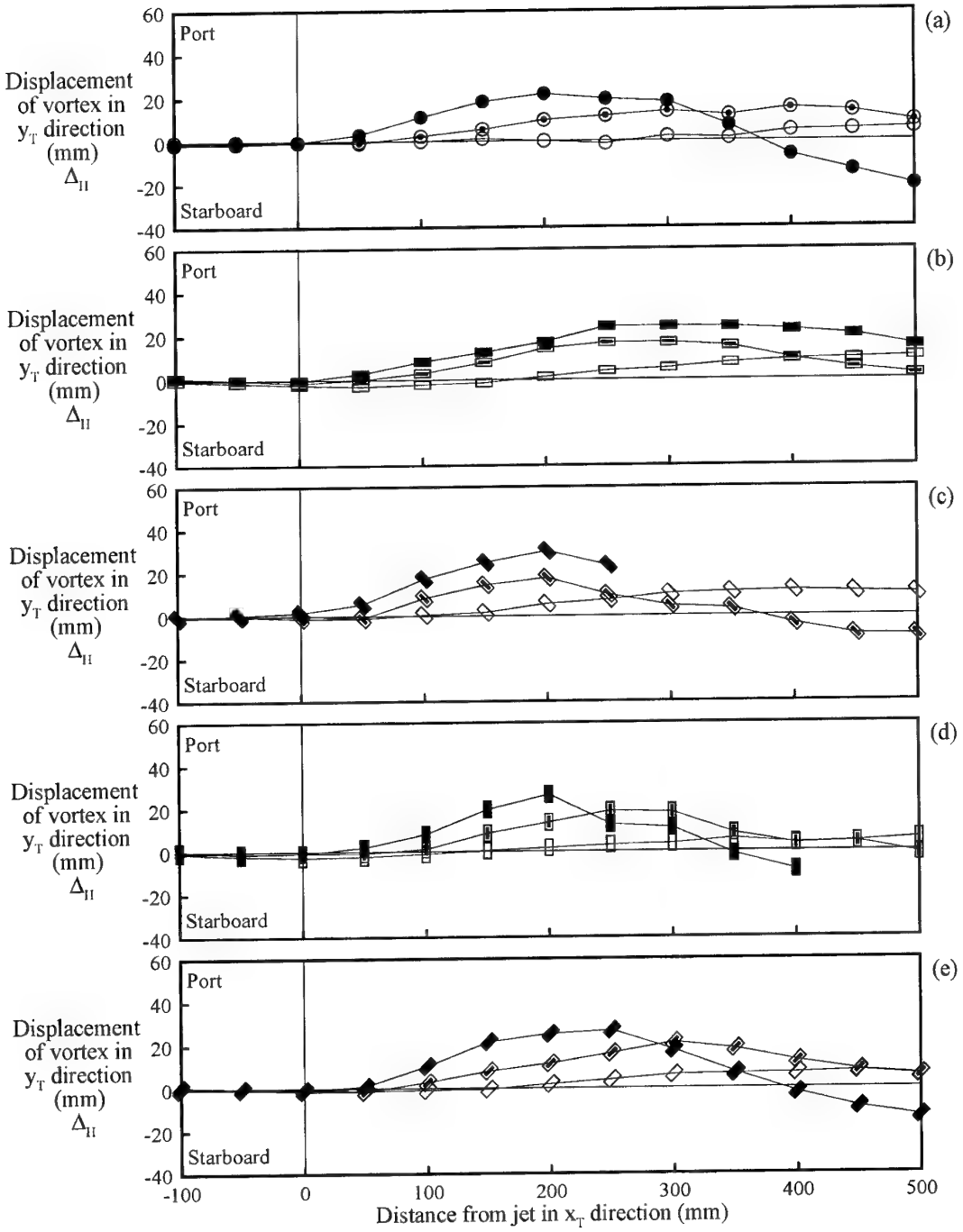

Figure 27. Effect of jet velocity on vortex displacement –plan views: (a) circular jet, pvj, θ = –90°; (b) rectangular jet ϕ = 0°, pvj, θ = 90°; (c) rectangular jet ϕ = 45°, pvj, θ = –90°; (d) rectangular jet ϕ = 90°, pvj, θ = 90°; (e) rectangular jet ϕ = 135°, pvj, θ = –90°. See Table 1 for an explanation of the symbols used for the different jets.

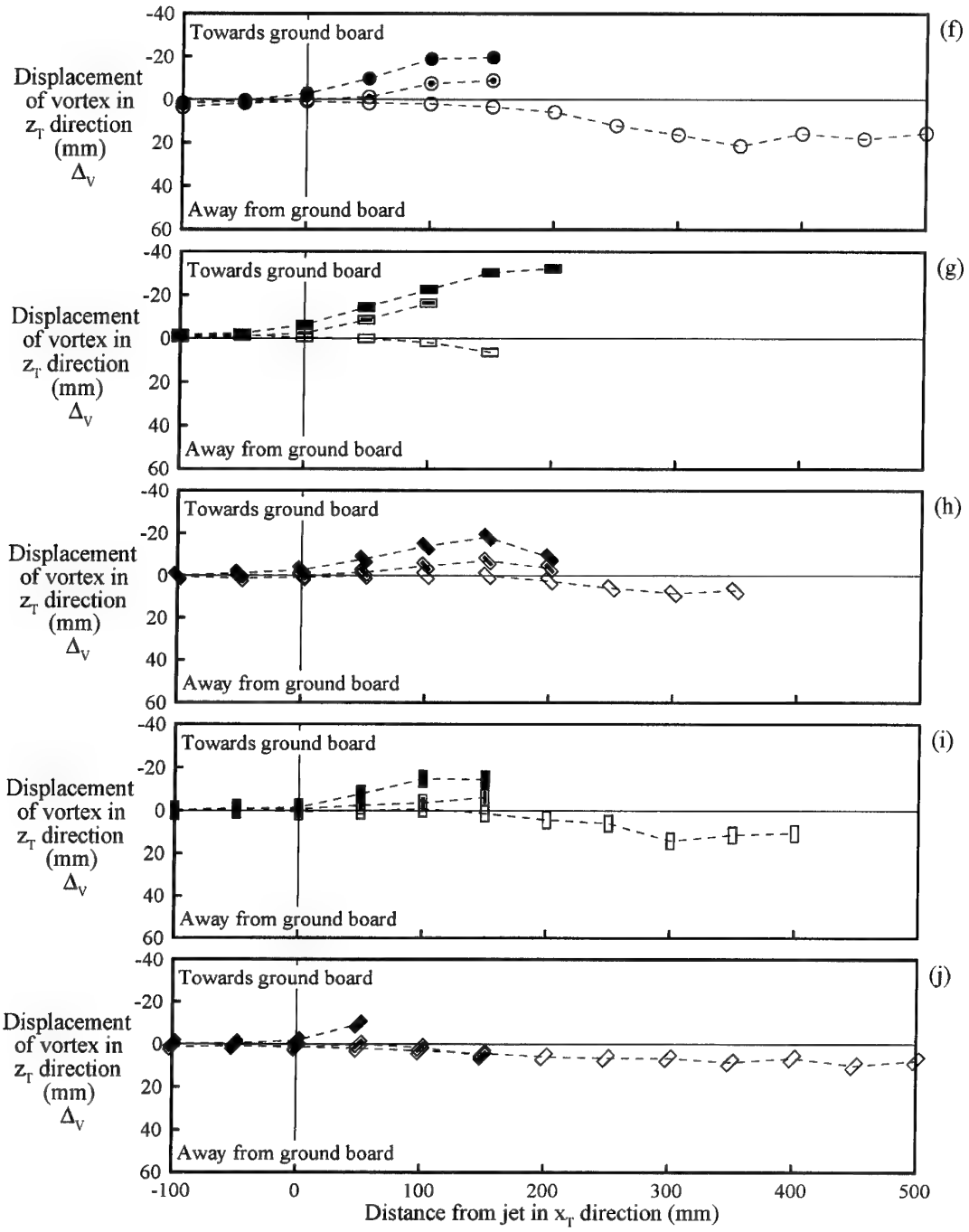

Figure 26 cont'd. Effect of jet velocity on vortex displacement –side views: (f) circular jet, cvj, θ = –90°; (g) rectangular jet ϕ = 0°, cvj, θ = 90°; (h) rectangular jet ϕ = 45°, cvj, θ = –90°; (i) rectangular jet ϕ = 90°, cvj, θ = –90°; (j) rectangular jet ϕ = 135°, cvj, θ = –90°. See Table 1 for an explanation of the symbols used for the different jets.

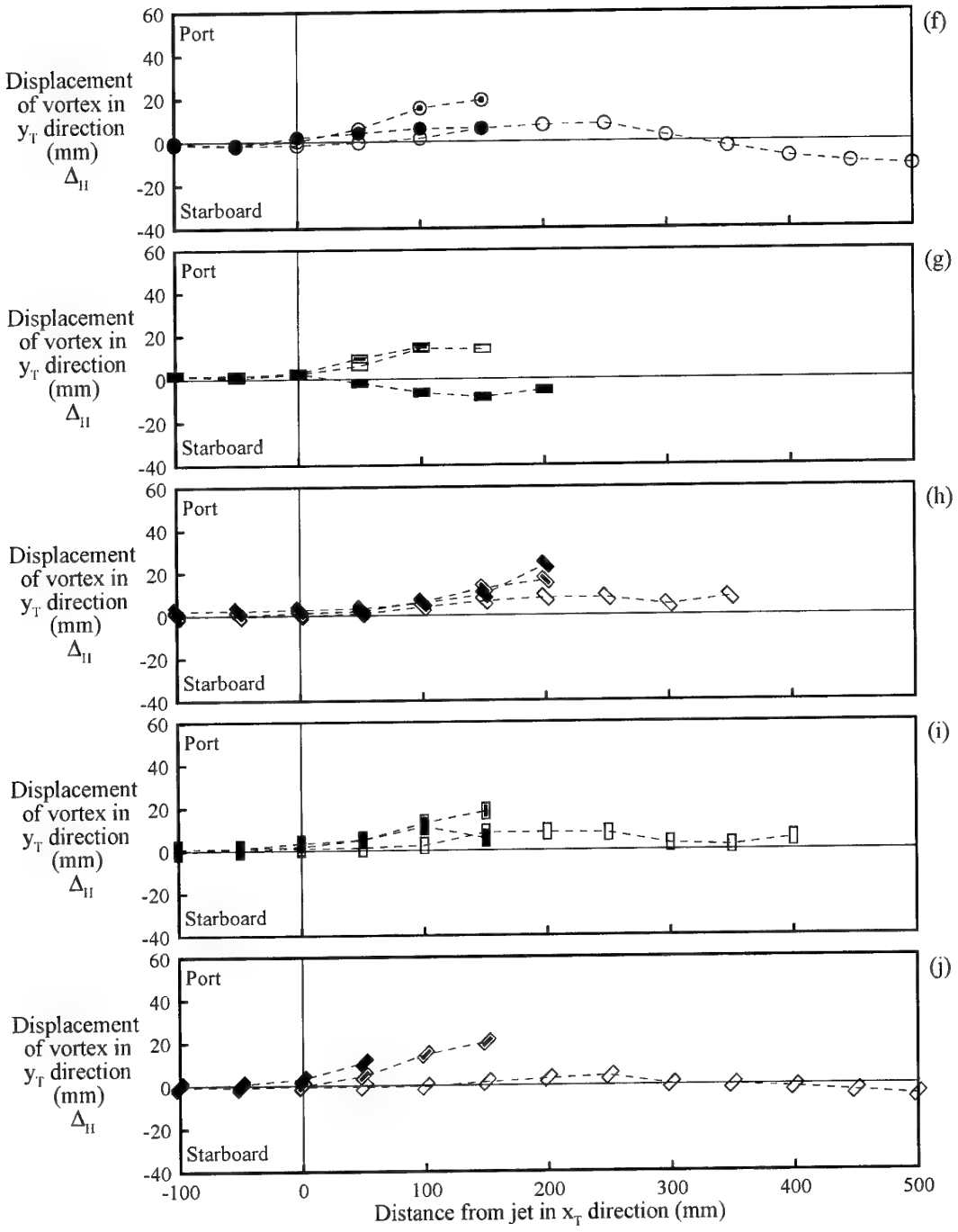

Figure 27 cont'd. Effect of jet velocity on vortex displacement –plan views: (f) circular jet, cvj, θ = –90°; (g) rectangular jet ϕ = 0°, cvj, θ = –90°; (h) rectangular jet ϕ = 45°, cvj, θ = –90°; (i) rectangular jet ϕ = 90°, cvj, θ = –90°; (j) rectangular jet ϕ = 135°, cvj, θ = –90°.
See Table 1 for an explanation of the symbols used for the different jets.

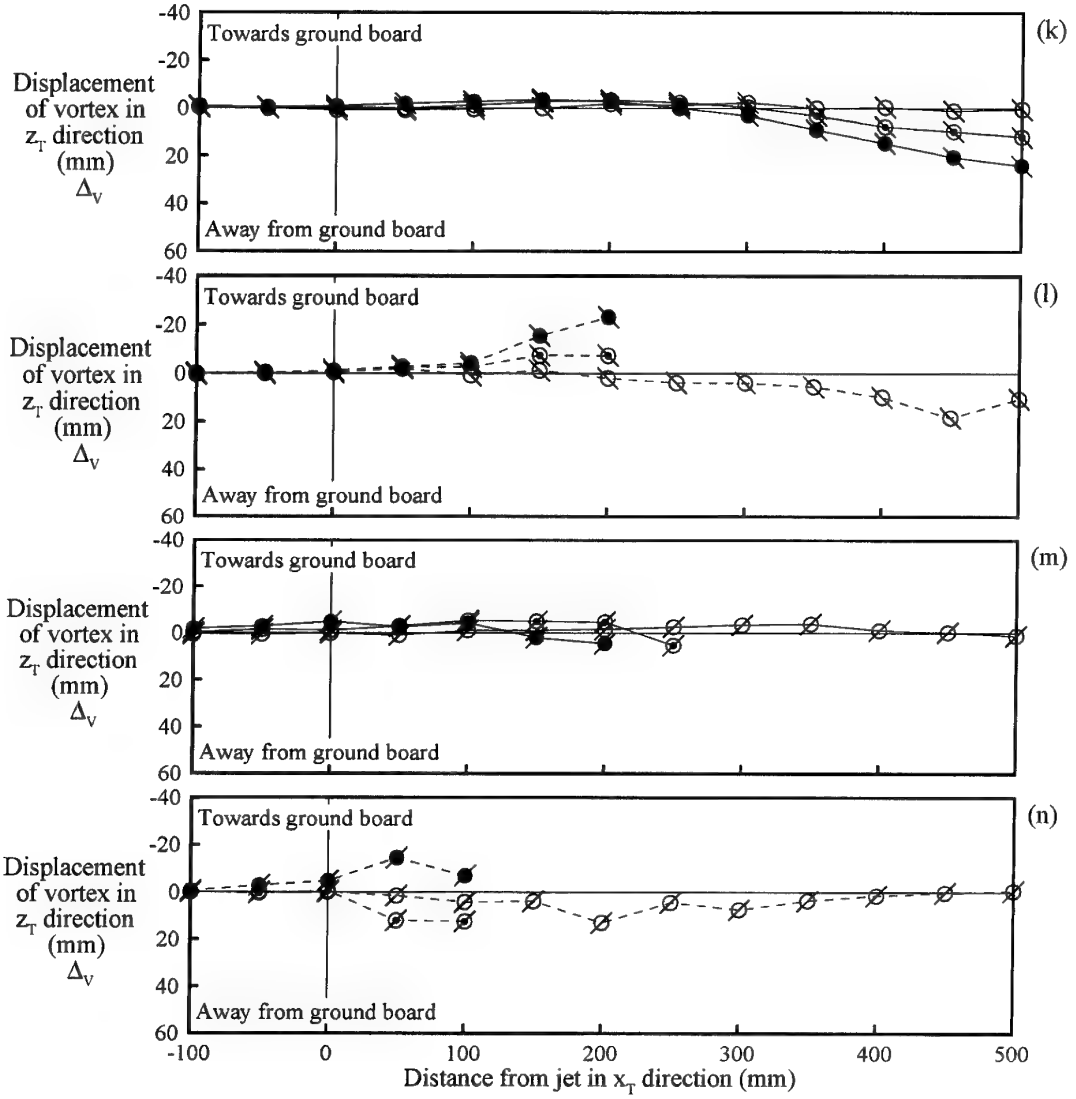

Figure 26 cont'd. Effect of jet velocity on vortex displacement – side views: (k) circular jet, pvj, θ = –45°; (l) circular jet, cvj, θ = –45°; (m) circular jet, pvj, θ = –135°; (n) circular jet, cvj, θ = –135°. See Table 1 for an explanation of the symbols used for the different jets.

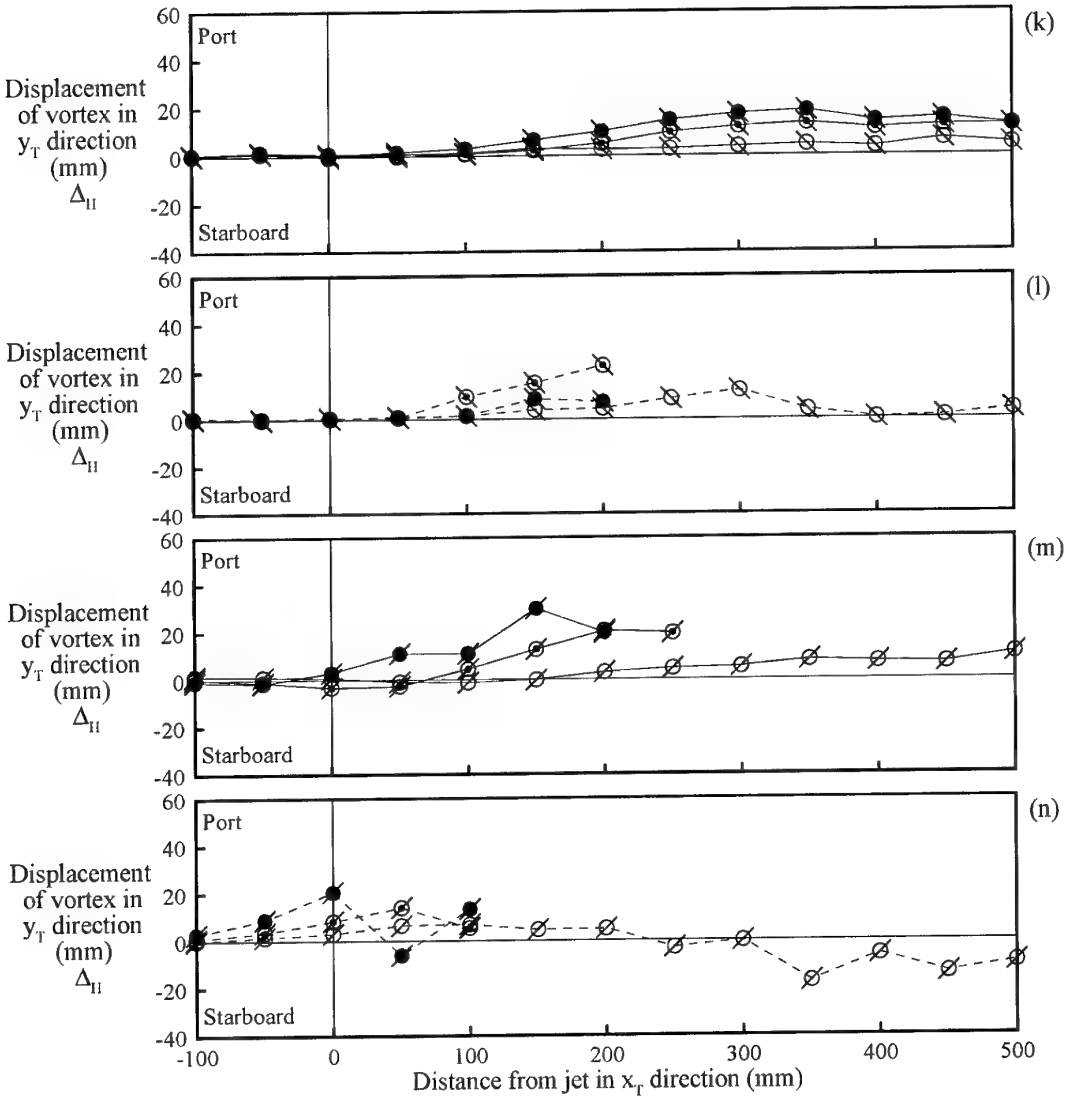

Figure 27 cont'd. Effect of jet velocity on vortex displacement: plan views. (k) circular jet, pvj, θ = –45°; (l) circular jet, cvj, θ = –45°; (m) circular jet, pvj, θ = –135°; (n) circular jet, cvj, θ = –135°. See Table 1 for an explanation of the symbols used for the different jets.

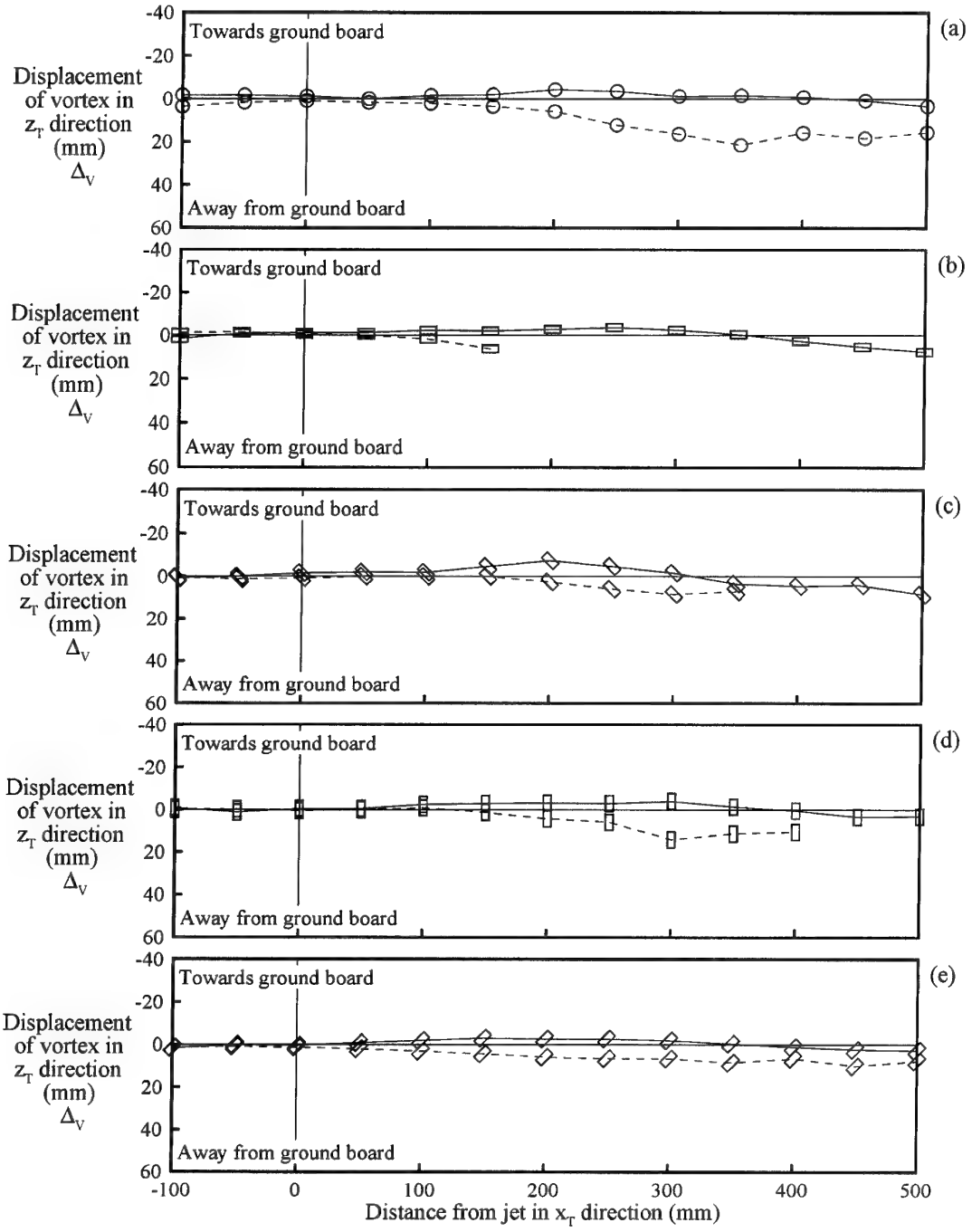

Figure 28. Effect of jet location on vortex displacement –side views: (a) circular jet, U_J = 0.4 m/s, θ = –90°; (b) rectangular jet ϕ = 0°, U_J = 0.4 m/s, θ = –90°; (c) rectangular jet ϕ = 45°, U_J = 0.4 m/s, θ = –90°; (d) rectangular jet ϕ = 90°, U_J = 0.4 m/s, θ = –90°; (e) rectangular jet ϕ = 135°, U_J = 0.4 m/s, θ = –90°. See Table 1 for an explanation of the symbols used for the different jets.

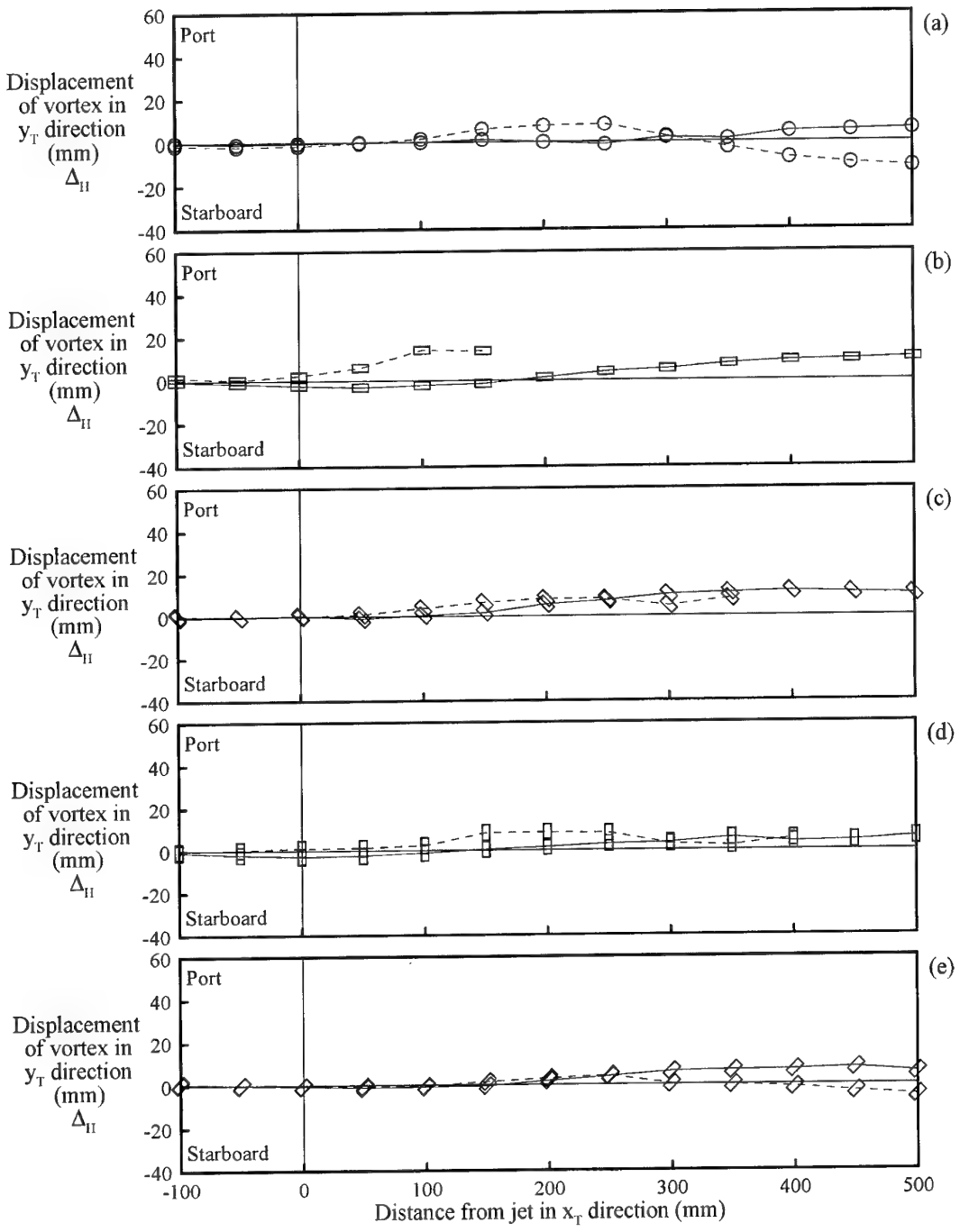

Figure 29. Effect of jet location on vortex displacement –plan views: (a) circular jet, U_J = 0.4 m/s, θ = –90°; (b) rectangular jet ϕ – 0°, U_J – 0.4 m/s, θ = –90°; (c) rectangular jet ϕ - 45°, U_J = 0.4 m/s, θ = –90°; (d) rectangular jet ϕ – 90°, U_J = 0.4 m/s, θ – -90°; (e) rectangular jet ϕ = 135°, U_J = 0.4 m/s, θ = -90°. See Table 1 for an explanation of the symbols used for the different jets.

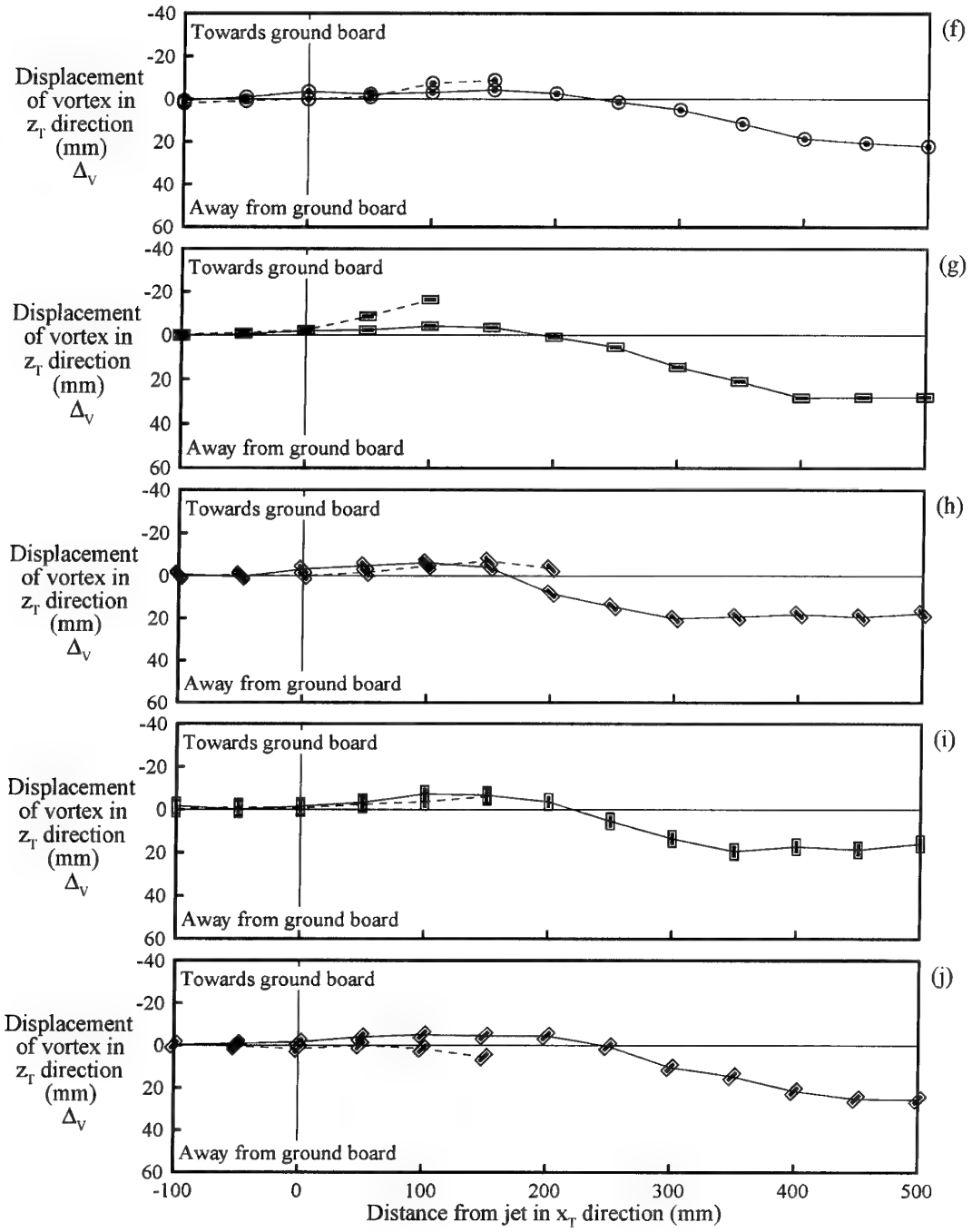

Figure 28 cont'd. Effect of jet location on vortex displacement side views: (f) circular jet, U_J = 0.8 m/s, θ = –90°; (g) rectangular jet ϕ = 0°, U_J = 0.8 m/s, θ = –90°; (h) rectangular jet ϕ = 45°, U_J = 0.8 m/s, θ = –90°; (i) rectangular jet ϕ = 90°, U_J = 0.8 m/s, θ = –90°; (j) rectangular jet ϕ = 135°, U_J = 0.8 m/s, θ = –90°.
See Table 1 for an explanation of the symbols used for the different jets.

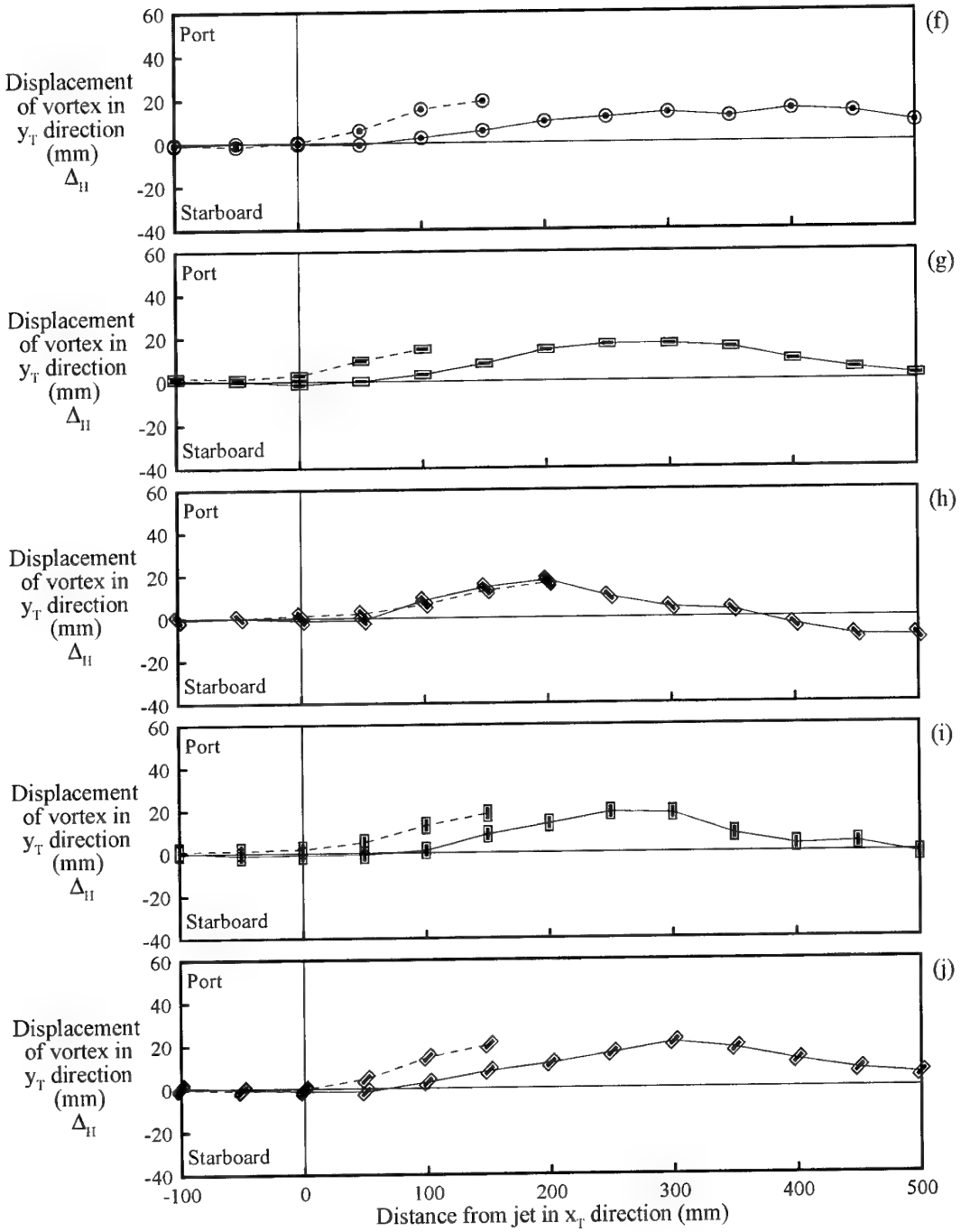

Figure 29 cont'd. Effect of jet location on vortex displacement plan views:
(f) circular jet, U_J = 0.8 m/s, θ = –90°; (g) rectangular jet ϕ = 0°, U_J = 0.8 m/s, θ = –90°;
(h) rectangular jet ϕ = 45°, U_J = 0.8 m/s, θ = –90°; (i) rectangular jet ϕ = 90°, U_J = 0.8 m/s, θ = –90°;
(j) rectangular jet ϕ = 135°, U_J = 0.8 m/s, θ = –90°.
See Table 1 for an explanation of the symbols used for the different jets.

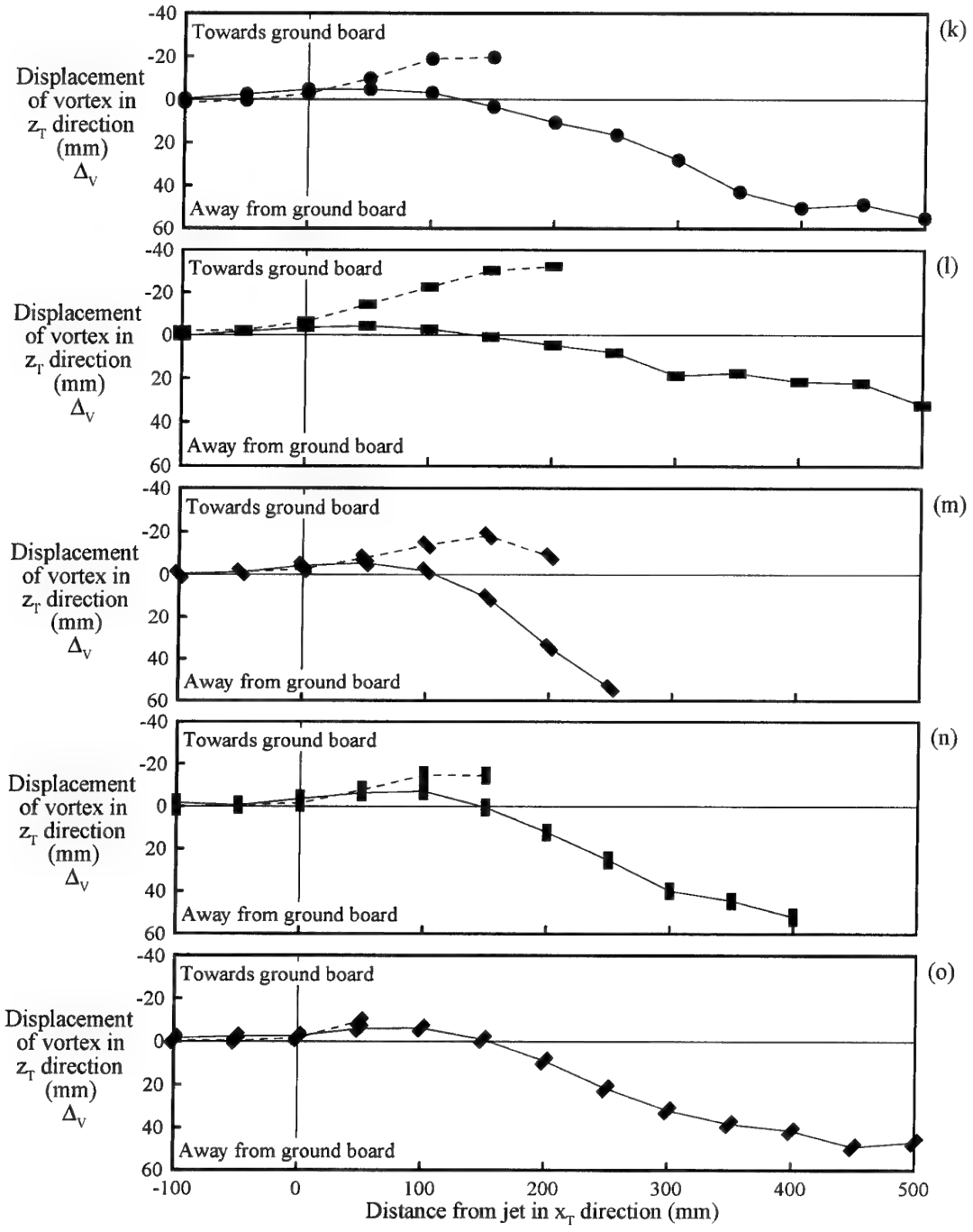

Figure 28 cont'd. Effect of jet location on vortex displacement side views: (k) circular jet, U_J = 1.2 m/s, θ = -90°; (l) rectangular jet ϕ = 0°, U_J = 1.2 m/s, θ = -90°; (m) rectangular jet ϕ = 45°, U_J = 1.2 m/s, θ = 90°; (n) rectangular jet ϕ = 90°, U_J = 1.2 m/s, θ = -90°; (o) rectangular jet ϕ = 135°, U_J = 1.2 m/s, θ = -90°. See Table 1 for an explanation of the symbols used for the different jets.

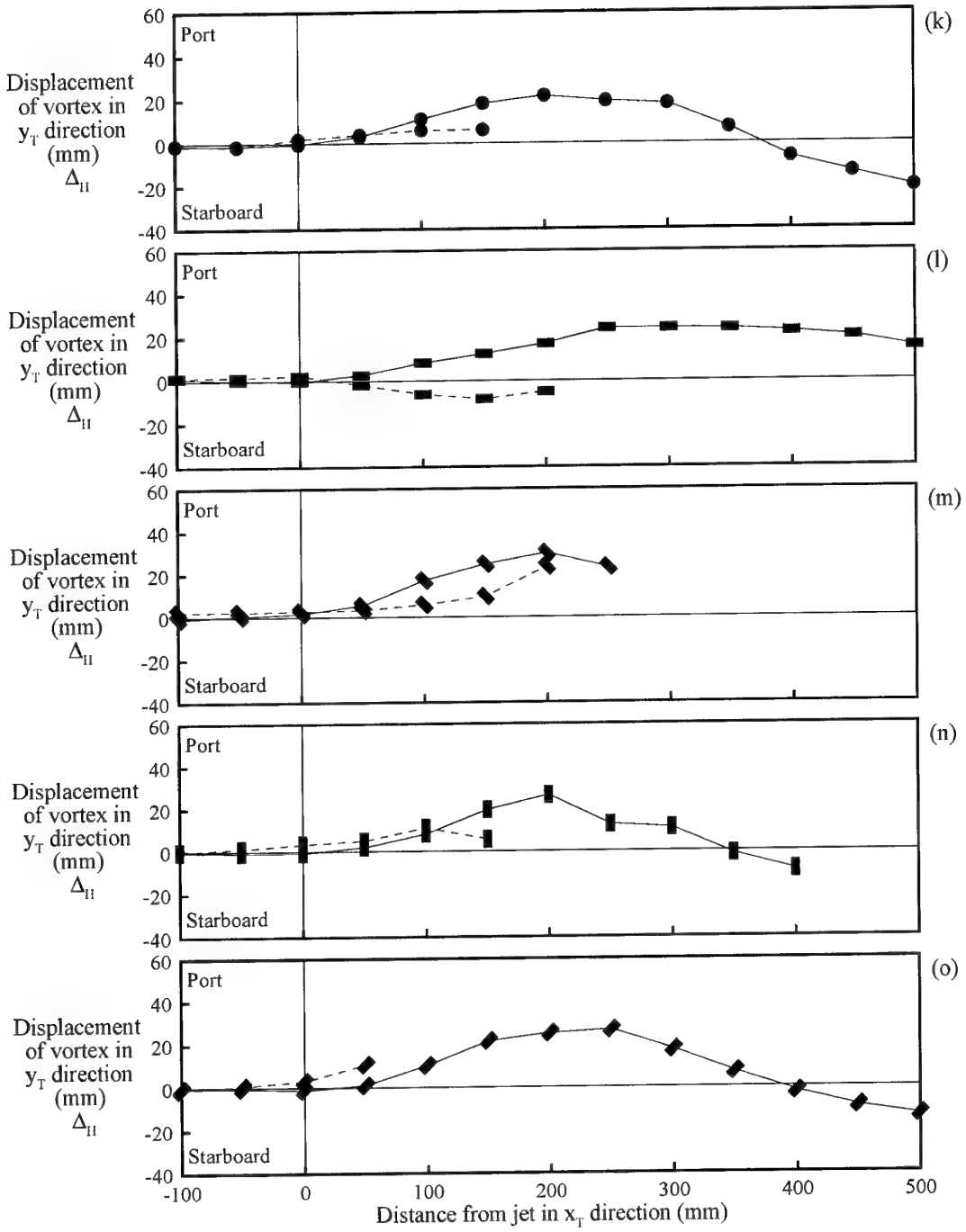

Figure 29 cont'd. Effect of jet location on vortex displacement plan views: (k) circular jet, U_J = 1.2 m/s, θ = -90°; (l) rectangular jet ϕ = 0°, U_J = 1.2 m/s, θ = -90°; (m) rectangular jet ϕ = 45°, U_J = 1.2 m/s, θ = –90°; (n) rectangular jet ϕ = 90°, U_J = 1.2 m/s, θ = -90°; (o) rectangular jet ϕ = 135°, U_J = 1.2 m/s, θ = –90°.
See Table 1 for an explanation of the symbols used for the different jets.

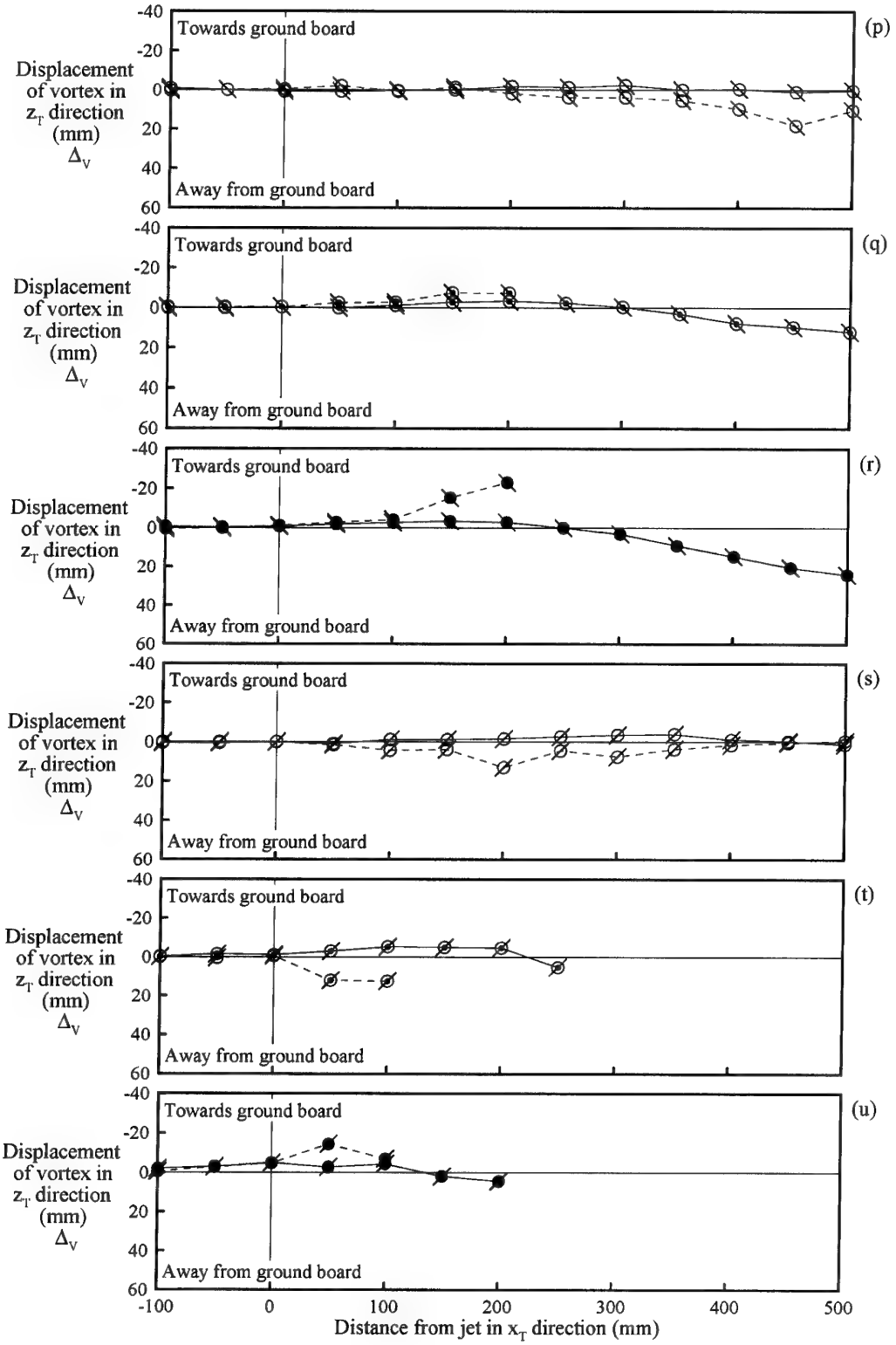

Figure 28 cont'd. Effect of jet location on vortex displacement –side views: (p) circular jet, U_J = 0.4 m/s, θ = –45°; (q) circular jet, U_J = 0.8 m/s, θ = –45°; (r) circular jet, U_J = 1.2 m/s, θ = –45°; (s) circular jet, U_J = 0.4 m/s, θ = –135°; (t) circular jet, U_J = 0.8 m/s, θ = –135°; (u) circular jet, U_J = 1.2 m/s, θ = –135° See Table 1 for an explanation of the symbols used for the different jets.

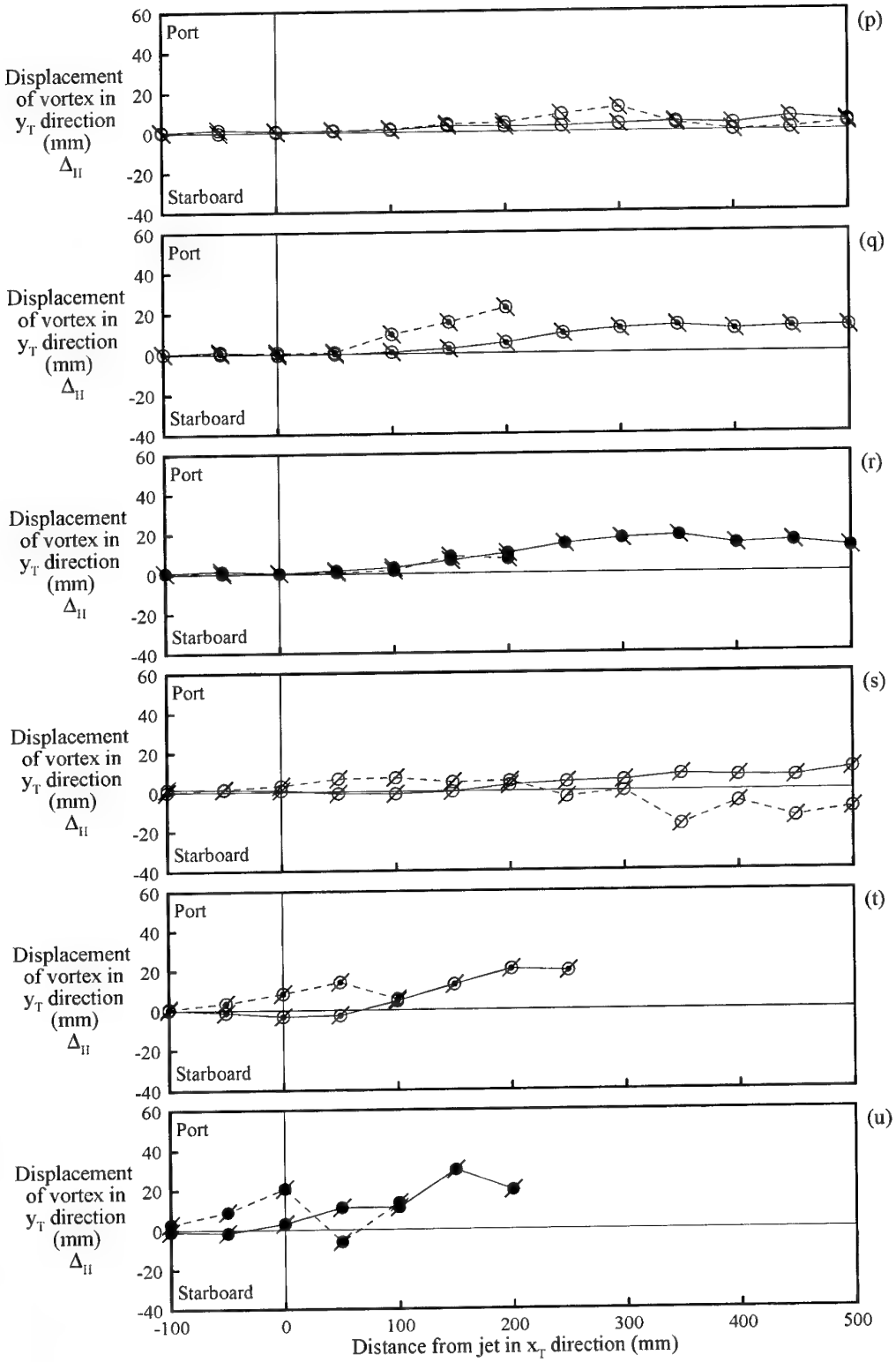

Figure 29 cont'd. Effect of jet location on vortex displacement –plan views: (p) circular jet, U_J = 0.4 m/s, θ = –45°; (q) circular jet, U_J = 0.8 m/s, θ = –45°; (r) circular jet, U_J = 1.2 m/s, θ = –45°; (s) circular jet, U_J = 0.4 m/s, θ = –135°; (t) circular jet, U_J = 0.8 m/s, θ = –135°; (u) circular jet, U_J = 1.2 m/s, θ = –135° See Table 1 for an explanation of the symbols used for the different jets.

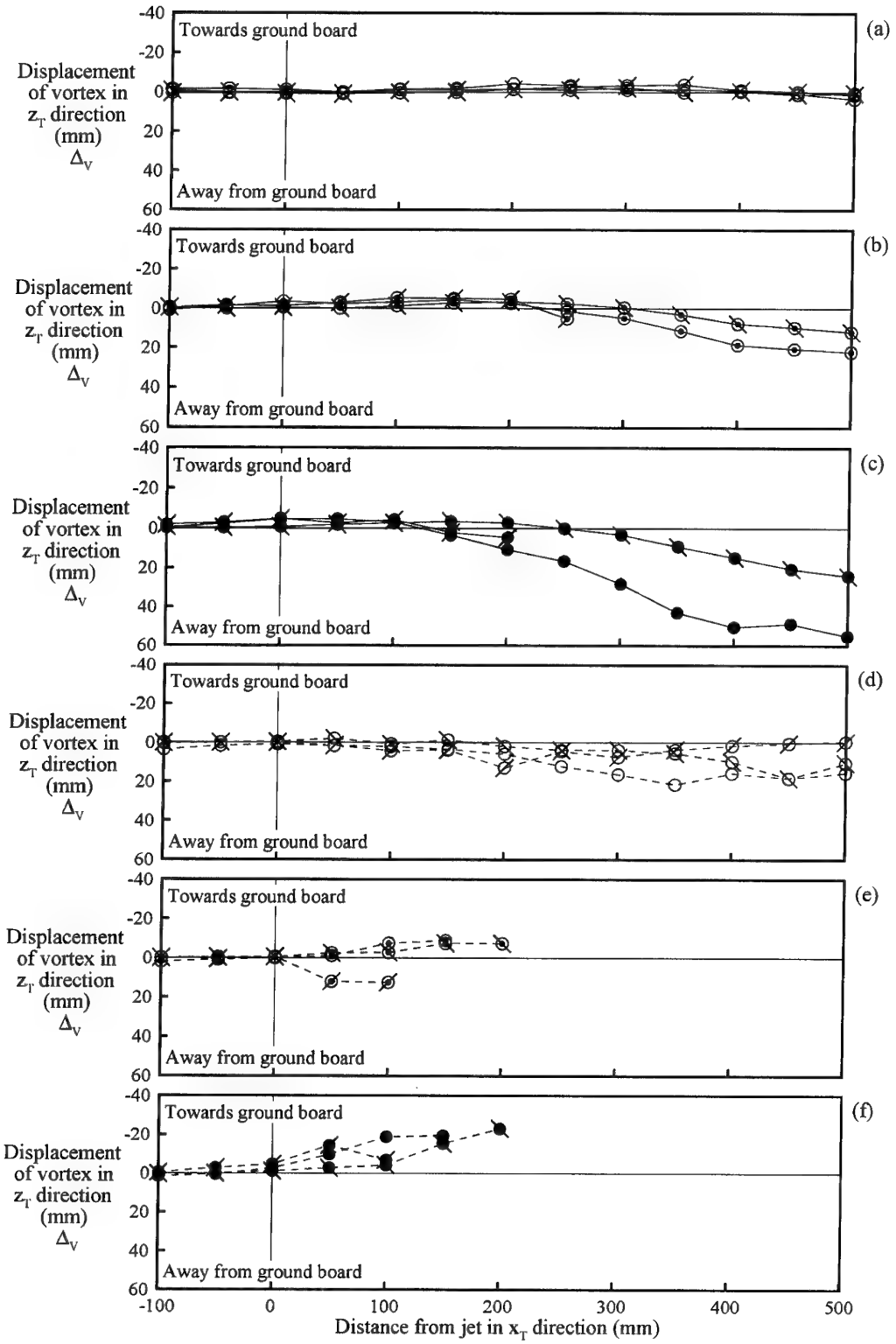

Figure 30. Effect of jet pitch angle on vortex displacement –side views: (a) circular jet, U_J = 0.4 m/s, pvj; (b) circular jet, U_J = 0.8 m/s, pvj; (c) circular jet, U_J = 1.2 m/s, pvj; (d) circular jet, U_J = 0.4 m/s, cvj; (e) circular jet, U_J = 0.8 m/s, cvj; (f) circular jet, U_J = 1.2 m/s, cvj. See Table 1 for an explanation of the symbols used for the different jets.

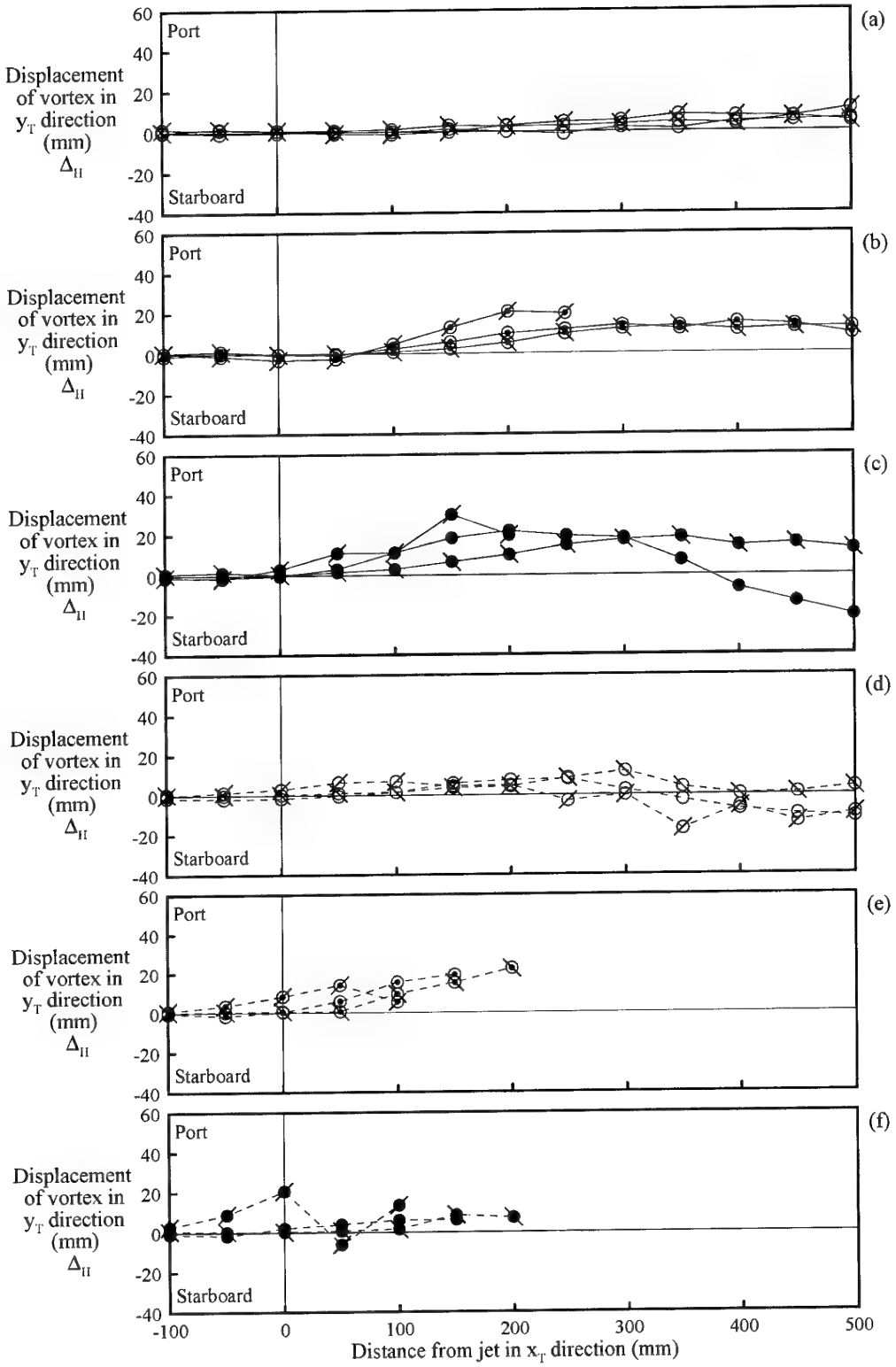

Figure 31. Effect of jet pitch angle on vortex displacement - plan views: (a) circular jet, U_J = 0.4 m/s, pvj; (b) circular jet, U_J = 0.8 m/s, pvj; (c) circular jet, U_J = 1.2 m/s, pvj; (d) circular jet, U_J = 0.4 m/s, cvj; (e) circular jet, U_J = 0.8 m/s, cvj; (f) circular jet, U_J = 1.2 m/s, cvj. See Table 1 for an explanation of the symbols used for the different jets.

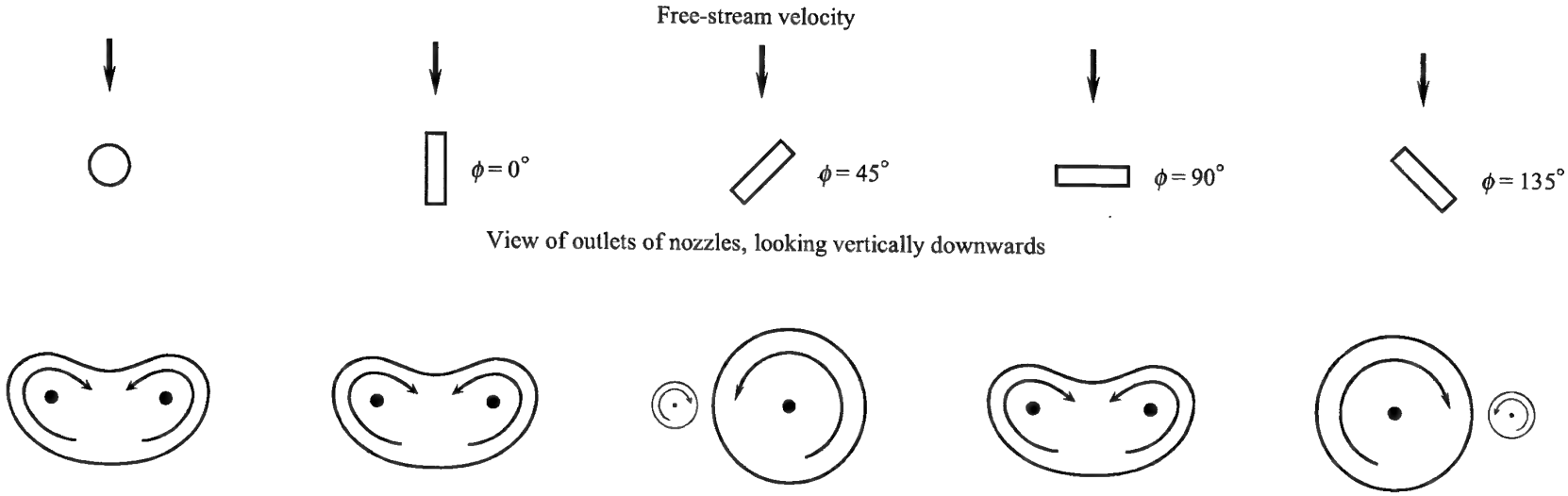

Figure 32. Details of the different nozzle shapes and corresponding transverse cross sections of the jets.

4.5.2 Effects of Jet Velocity

Three different jet velocities were used in the current investigation, namely $U_J = 0.4$, 0.8 and 1.2 m/s. These three jet velocities were chosen since the location of the curved jets near the nozzle outlet ($x_T < 100$ mm) generally varied from being initially above the main vortex to being initially below the main vortex –see Figures 12 to 17.

Figures 26 and 27 show that jet velocity has a significant effect on vortex displacement. Considering the Δ_V data, the behaviour of vortices perturbed by pro-vortex jets is different from that for vortices perturbed by contra-vortex jets. At $U_J = 0.4$ m/s, pro-vortex jets generally cause vortices to move slightly towards the ground board (Figures 26 a to e, for example), whereas contra-vortex jets generally cause vortices to move away from the ground board (Figures 26 f to j, for example). As U_J increases, the pro-vortex jets generally cause the vortices to move progressively away from the ground board, whereas the contra-vortex jets generally cause the vortices to move progressively towards the ground board. For $U_J = 1.2$ m/s, the vortices perturbed by the pro-vortex jets are generally further away from the ground board and the vortices perturbed by the contra-vortex jets are generally closer to the ground board, compared with their initial unperturbed locations in both cases. Vortices can be destroyed as a result of increasing the jet velocity. Vortices are destroyed at or beyond $x_T = 200$ mm ($x_T/D \approx 30$) by contra-vortex jets having $U_J = 0.8$ and 1.2 m/s. Possible physical reasons for this are given in Section 4.5.3. Considering the Δ_H data, vortices are generally displaced towards port for all three values of U_J. The data associated with the pro-vortex jets follow a general trend in which the peaks of the curves correspond to higher positive values of Δ_H (movement of vortices to port), and occur at lower values of x_T, as U_J increases. The Δ_H data associated with the contra-vortex jets follow a similar trend, except for $U_J = 1.2$ m/s, where the peaks of the curves are not well defined and generally correspond to lower values of Δ_H than for $U_J = 0.8$ m/s.

Jet/vortex interactions using jets having $U_J > 1.2$ m/s were observed, but are not reported here since the jet flows deflected off the floor of the tunnel, back into the cross-flow, and introduced extraneous disturbances into the flow. In these cases, the jet cores had by-passed the outer-flow region of the vortex before they were significantly deflected in the downstream direction, so that there was minimal interaction between the jets and the vortex. The cases are of interest since they show that too great a jet velocity is as ineffective as too small a jet velocity.

4.5.3 Effects of Jet Location

Two different jet locations were used in the current investigation. The origin of the jet coordinate system was located at either 50 mm ($x_T/D \approx 7.5$) to port of an unperturbed vortex, i.e. $x_T = 0$, $y_T = 50$, $z_T = 0$ mm (pro-vortex jet), or at 50 mm to starboard of an unperturbed vortex, i.e. $x_T = 0$, $y_T = -50$, $z_T = 0$ mm (contra-vortex jet).

Figures 28 and 29 show that the location of a jet has a significant effect on vortex behaviour. The most obvious feature of the plots is that contra-vortex jets often destroy the vortex, particularly jets having $U_J = 0.8$ and 1.2 m/s. The reason for this is that contra-vortex jets oppose the vortex circumferential velocity and destroy the vortex by reducing its angular momentum. Ligrani & Schwartz (1990) found that the most significant alterations to vortex structure were obtained when the jet flow close to the nozzle outlet opposed the vortex circumferential velocity. Conversely, pro-vortex jets aid the vortex circumferential velocity, and the vortex is generally not destroyed by these jets. Figure 28 shows that jet location often has a marked effect on values of Δ_V. For $U_J = 0.4$ m/s, pro-vortex jets have little effect on vortex movement towards or away from the ground board (Figures 28 a to e, for example). For $U_J = 0.8$ and 1.2 m/s, pro-vortex jets generally cause vortices to move away from the ground board (Figures 28 f to o, for example). Contra-vortex jets have a variable effect on vortices depending on the jet velocity. For $U_J = 0.4$ m/s, contra-vortex jets cause vortices to move away from the ground board (Figures 28 a to e, for example). As U_J increases, the contra-vortex jets cause the vortices to move back towards the ground board (Figures 28 f to o, for example) and for $U_J = 1.2$ m/s the vortices are closer to the ground board than their initial unperturbed locations. Despite the above fundamental differences in the jet/vortex interaction for pro-vortex and contra-vortex jets, the Δ_H data in Figure 29 shows that both pro-vortex and contra-vortex jets generally cause vortices to move towards port for all jet velocities.

The reasons for the vortices always moving to port are unclear, but the behaviour can possibly be explained by referring to Figures 18 to 23, which depict idealised vortex behaviour. It may seem logical that if a pro-vortex jet causes the longitudinal vortex to move in one direction, then a contra-vortex jet should cause the vortex to move in the opposite direction. However, an examination of Figures 18 to 23 indicates that the initial vortex displacement ($x_T \approx 100$ mm, $x_T/D \approx 15$) is predominantly to port for both pro-vortex jets and contra-vortex jets. The reason for this is that the angular positions of the jets relative to the longitudinal vortex are different for the two cases. For the pro-vortex jet case, the jet vortices are further away from the ground board than for the contra-vortex jet case due to the rotating action of the longitudinal vortex. The rotating flow field prevents the contra-vortex jet from moving sufficiently far away from the ground board to cause major movement of the longitudinal vortex to starboard. Although the longitudinal vortex may move to starboard further downstream, there is generally not a large overall movement to starboard.

4.5.4 Effects of Jet Pitch Angle

Three different jet pitch angles were used in the current investigation, namely $\theta = -45°$ (jet velocity initially inclined downstream), $\theta = -90°$ (jet velocity initially inclined normal to the cross flow), and $\theta = -135°$ (jet velocity initially inclined upstream). Jet pitch angles were only varied for the circular jets.

Figures 30 and 31 show that, for $U_J = 0.4$ m/s, jet pitch angle does not have a large effect on vortex behaviour. At this jet velocity, the jets are dominated by the cross flow and they are quickly swept downstream as they enter the cross flow, reducing any influence of different jet pitch angles. For both pro-vortex and contra-vortex jets having $U_J = 0.8$ and 1.2 m/s, jets pitched at $\theta = -135°$ destroyed the vortex at smaller values of x_T than jets pitched at $\theta = -45°$ and $-90°$, where vortex destruction occurred. This can possibly be explained by the fact that the jets inclined upstream interacted earlier with the vortex than for the other cases. The upstream flows of these jets opposed the flow of the oncoming vortex, making the vortex unstable and leading to its early destruction.

4.5.5 Jet Configurations Giving Largest Vortex Displacements

As an outcome of the investigation, it is possible to indicate which jet configurations give the maximum horizontal and vertical lateral displacements. The findings can be used as guidelines in possible future aircraft control work. Lateral displacements will be compared at $x_T = 200$ mm ($x_T/D \approx 30$), downstream of the outlets of the nozzles. This x_T location is near the midpoint of the x_T range considered, and also vortices were often destroyed at greater downstream distances. The jet configurations giving the largest and the second largest vortical displacements in each of the four different lateral directions are compared in Table 2.

Table 2. Vortex displacements in four different lateral directions at $x_T = 200$ mm ($x_T/D \approx 30$). Rows 1 to 4: Largest displacements. Rows 5 to 8: Second largest displacements.

Direction	Jet and symbol	Line connecting symbol	Jet velocity U_J (m/s)	Roll angle ϕ (degrees)	Pitch angle θ (degrees)	Jet location y_T (mm)	Vortex Displacement
Away from ground board	Rectangular jet ◆	——	1.2	45	–90	50 (pvj*)	+34.4 mm $\Delta_V/D = +5.4$
Towards ground board	Rectangular jet ■	- - - - -	1.2	0	–90	50 (cvj*)	–32.2 mm $\Delta_V/D = -5.0$
Towards port	Rectangular jet ◆	——	1.2	45	–90	50 (pvj)	+30.0 mm $\Delta_H/D = +4.7$
Towards starboard	Rectangular jet ■	- - - - -	1.2	0	–90	50 (cvj)	–5.3 mm $\Delta_H/D = -0.8$
Away from ground board	Circular jet ∅	- - - - -	0.4		–135	50 (cvj)	+13.0 mm $\Delta_V/D = +2.0$
Towards ground board	Circular jet ●	- - - - -	1.2		–45	50 (cvj)	–23.1 mm $\Delta_V/D = -3.6$
Towards port	Rectangular jet ▮	——	1.2	90	–90	50 (pvj)	+26.5 mm $\Delta_H/D = +4.1$
Towards starboard	Circular jet ○	——	0.4		–90	50 (pvj)	0.0 mm $\Delta_H/D = 0.0$

*pvj = pro-vortex jet; cvj = contra-vortex jet.

Table 2 shows that the maximum lateral vortex displacements in the four transverse directions are obtained using just two different jet configurations, namely a pro-vortex rectangular jet having a velocity of 1.2 m/s and a roll angle of 45°, and a contra-vortex rectangular jet having a velocity of 1.2 m/s and a roll angle of 0°. The first jet causes maximum vortex displacement both away from the ground board and towards port, and the second jet causes maximum vortex displacement both towards the ground board and towards starboard. The maximum vortex displacements in the directions away from the ground board, towards the ground board and towards port are all approximately the same, but the maximum displacement towards starboard is less than 20% of the other three displacements. This may pose some problems when controlling vortical flow over an aircraft, since a vortex can primarily only be moved laterally across a surface in one direction at this x_T location irrespective of whether a pro-vortex or contra-vortex controlling jet is used. Possible reasons for this behaviour are given in Section 4.5.3. Table 2 shows that there are no clear patterns in the jet configurations giving the second most maximum vortex lateral displacements. The maximum vortex displacements in the directions away from the ground board, towards the ground board and towards port are 2.6 times, 1.4 times and 1.1 times respectively the second most maximum vortex displacements in these three directions. No meaningful comparison can be made for displacements towards starboard since the second most maximum displacement towards starboard was 0.0 mm.

Vortex lateral displacement is not the only criterion to consider when assessing the effectiveness of a given jet flow. In some control situations, jet configurations that destroy vortices may be important. From Figures 24 and 25 (for example) it can be seen that a contra-vortex rectangular jet having a velocity of 1.2 m/s and a roll angle of 135° is the most efficient jet at destroying the vortex, i.e. the vortex is destroyed at the least downstream distance from the nozzle.

The foregoing suggests that it may be possible to achieve wide-ranging aircraft control by locating a rectangular nozzle on either side of a vortex, such that the nozzles can be rolled to any desired angle and used independently or simultaneously. The mechanical arrangement could be uncomplicated and would make best use of any limited supply of jet fluid.

5. Concluding Remarks

An experimental parametric study has been undertaken in the AMRL flow-visualization water tunnel to determine how vortices are affected by different types of jet flows. The study is the first stage of an investigation aimed at determining how flow through ducts in aircraft lifting surfaces away from the forebody can be used to manipulate vortical flow over modern high-performance aircraft to modify the loading on the aircraft and thus improve aircraft control at extreme flight attitudes. An undisturbed vortex generates some form of pressure distribution on an aircraft surface and the aim is to

modify the pressure distribution for control purposes by changing the position and/or magnitude of the vortex, or by destroying the vortex. To determine which jet flows are the best to use to modify the vortical flow, vortex behaviour was examined for 42 different jets, using dye to visualize the jet and vortex flows. Jet shape, jet velocity, jet location and jet pitch angle were all varied and had different effects on vortex behaviour. It is not possible at this stage to say whether the observed modified vortical flows can be utilised to improve aircraft control and further experiments (see below) will be necessary to assess the effects of the different jets. However, the experiments to date provide some guidelines on the direction to proceed in any future work on aircraft control.

Circular and rectangular nozzles were used to produce the jets and it was found that jet shape had a significant effect on vortex behaviour. Jets emerging from the rectangular nozzle set at different roll angles, ϕ, had different vortical flow structures (see below) and produced a relative large range of lateral displacement of the vortex.

Jet velocity ratios of 4, 8 and 12 were used in the study and it was found that jet velocity had a significant effect on vortex behaviour. Vortex lateral displacement was generally found to increase with increasing jet velocity, suggesting that a wider range of control could be obtained by simply increasing the supply of high-pressure fluid to generate faster jets. However, it was found that for high jet velocities, the jet bypassed the vortex with little interaction, so that too strong a jet may be just as ineffective as too weak a jet from the point of view of control.

The lateral location of the jet relative to the vortex was found to have a significant effect on vortex behaviour. It was found that contra-vortex jets, i.e. jets that opposed the vortex circumferential velocity, often destroyed the vortex by reducing its angular momentum. Conversely, pro-vortex jets aided the vortex circumferential velocity, and the vortex was generally not destroyed by these jets. It may be possible to obtain improved aircraft control by using jet flows to degrade the flow over the aircraft, such as by destroying a vortex over one of the aircraft wings to remove a region of low pressure, and thus obtain asymmetrical rolling moments on the aircraft.

Three different jet pitch angles, θ, were used for the circular jet, namely $\theta = -45°, -90°$ and $-135°$, and one jet pitch angle was used for the rectangular jet, namely $\theta = -90°$. For the circular jet, it was found that different jet pitch angles generally did not have a large effect on vortex behaviour, although jets pitched at $\theta = -135°$ were more effective in destroying a vortex than jets pitched at $\theta = -45°$ and $-90°$.

The jet configurations that gave the greatest vortex lateral displacements downstream of the nozzle (within say about 30 nozzle diameters or equivalent diameters for the rectangular jet) are of interest since they provide the maximum control effect for a given available jet mass flow rate. It was found that a pro-vortex rectangular jet having a velocity of 1.2 m/s and a roll angle of 45° caused the maximum vortex displacement away from the ground board and also towards port. It was also found that a contra-

vortex rectangular jet having a velocity of 1.2 m/s and a roll angle of 0° caused the maximum vortex displacement towards the ground board and also towards starboard. In addition, it was found that a contra-vortex rectangular jet having a velocity of 1.2 m/s and a roll angle of 135° caused the vortex to be destroyed at the smallest downstream distance from the nozzle.

Possible reasons for the rectangular jets giving the above extremes of control effect were investigated. Flow-visualization experiments were carried out using the rectangular nozzle set different roll angles to observe the flow structure of the jets. It was found that when the jet flows were symmetrical with the cross flow, which occurred when the rectangular nozzle was set at roll angles of 0° and 90°, the jets were comprised of a pair of symmetrical counter-rotating vortices. However, for asymmetrical jet flows, which occurred when the rectangular nozzle was set at roll angles of 45° and 135°, the jets were comprised of a strong dominant vortex and a very weak counter-rotating vortex. When the rectangular nozzle was set at $\phi = 45°$, the dominant vortex rotated in an anti-clockwise direction when looking upstream, and conversely for the $\phi = 135°$ case. The lateral spread of the jets was also different for the different roll angles of the rectangular nozzle.

The foregoing suggests that it may be possible to achieve wide-ranging aircraft control by locating a rectangular nozzle on either side of a vortex, such that the nozzles can be rolled to any desired angle and used independently or simultaneously.

For the next stage of the investigation, it is planned to carry out jet/vortex flow-visualization experiments in the water tunnel using a generic model of a high-performance aircraft to generate the jets and the vortices. Jet flows will be produced by water flowing through ducts from the high-pressure side to the low-pressure side of aircraft lifting surfaces away from the forebody of the aircraft, so that the system would be simple with no bulky hardware. The interaction between aircraft vortices and jet flows will be examined in an attempt to determine the jet/vortex cases most likely to improve aircraft control at extreme flight attitudes. The findings of the initial experimental study, referred to above, will be used as a guide when setting up the experimental program so that only the important jet cases are tested.

6. Acknowledgements

The author is grateful for help received from Dr D. H. Thompson, Head Aerodynamics Applications, and from Mr I. D Amott and Mr D. M. Carnell, who assisted with the experimental program.

7. References

Fric, T. F. 1990, 'Structure in the near field of the transverse jet.' PhD thesis, California Institute of Technology, California, USA.

Fric, T. F. & Roshko, A. 1991, 'Structure in the near field of the transverse jet.' In *Turbulent Shear Flows 7*, Selected Papers from the Seventh International Symposium on Turbulent Shear Flows, Stanford University, USA, August 21-23, 1989, Editors: Durst, F., Launder, B. E., Reynolds, W. C., Schmidt, F. W. & Whitelaw, J. H., Springer-Verlag, Berlin, Heidelberg.

Fric, T. F. & Roshko, A. 1994, 'Vortical structure in the wake of a transverse jet.' *Journal of Fluid Mechanics*, Vol. 279, pp. 1-47, Cambridge University Press, Cambridge, UK.

Hunsaker, J. C. & Rightmire, B. G. 1947, 'Engineering applications of fluid mechanics.' McGraw Hill Book Company, New York, USA.

Jacob, J.D., Liepmann, D. & Savas, Ö. 1995, 'Experimental investigation of the trailing vortex wake of a rectangular wing'. *AIAA-95-1841-CP*, 13th AIAA Applied Aerodynamics Conference, San Diego, CA, USA, June 19-22, pp. 640-646.

Johnston, J. P. & Nishi, M. 1990, 'Vortex generator jets –means for flow separation control'. *AIAA Journal*, Vol. 28, No. 6, pp. 989-994.

Kelso, R. M., Lim, T. T. & Perry, A. E. 1996, 'An experimental study of round jets in cross-flow.' *Journal of Fluid Mechanics*, Vol. 306, pp. 111-144.

Ligrani, P. M. & Schwartz, G. E. 1990, 'Control of embedded longitudinal vortices using a wall jet'. *International Journal of Heat and Fluid Flow*, Vol. 11, No. 4, pp. 274-283.

Scorer, R. S. 1958, 'Natural Aerodynamics', Pergamon Press.

Shah, G. H. & Clemons, S. B. 1995, 'Parametric wind-tunnel investigation of high-alpha aerodynamic and stability characteristics of a prototype F–18E configuration.' *AIAA-95-3503, Atmospheric Flight Mechanics Conference*, Baltimore, Maryland, USA, August 7-9.

Walker, L. 1993, 'Why the F–15 rolls right at high angles of attack'. *McDonnell Douglas Aerospace Digest*, 1-5, December.

Zhang, X. & Collins, M. W. 1997, 'Measurements of a longitudinal vortex generated by a rectangular jet in a turbulent boundary layer.' *Physics of Fluids*, Vol. 9, pp. 1665-1673.

DISTRIBUTION LIST

A Parametric Study of Jet/Vortex Interactions
in the AMRL Water Tunnel

Lincoln P. Erm

AUSTRALIA

DEFENCE ORGANISATION

Task Sponsor

S&T Program

Chief Defence Scientist
FAS Science Policy
AS Science Corporate Management
Director General Science Policy Development
} shared copy

Counsellor Defence Science, London (Doc Data Sheet only)
Counsellor Defence Science, Washington (Doc Data Sheet only)
Scientific Adviser to MRDC Thailand (Doc Data Sheet only)
Scientific Adviser Joint
Navy Scientific Adviser (Doc Data Sheet and distribution list only)
Scientific Adviser - Army (Doc Data Sheet and distribution list only)
Air Force Scientific Adviser
Director Trials

Aeronautical and Maritime Research Laboratory

Chief of Air Operations Division
Research Leader Avionics and Flight Mechanics, N. Pollock
Head Aerodynamic Applications, D. H. Thompson
Head Flight Mechanics, N. Matheson
Head Flight Dynamics Applications, J. S. Drobik
Author, L. P. Erm (10 copies)

V. Baskaran
R. Blyth
J. C. Clayton
M. Giacobello
S. S. Lam
H. A. Quick
A. H. Blandford
D. M. Carnell
G. S. Dietachmayer
A. A. Gonzalez
P. T. Malone

DSTO Library and Archives

Library Fishermans Bend
Library Edinburgh
Australian Archives

US Defense Technical Information Center, 2 copies
UK Defence Research Information Centre, 2 copies
Canada Defence Scientific Information Service
NZ Defence Information Centre

Capability Systems Staff
Director General Maritime Development (Doc Data Sheet only)
Director General Aerospace Development (Doc Data Sheet only)

Knowledge Staff
Director General Command, Control, Communications and Computers (DGC4) (Doc Data Sheet only)

Army
ABCA National Standardisation Officer, Puckapunyal (4 copies)
SO (Science), Deployable Joint Force Headquarters (DJFHQ) (L), Enoggera QLD (Doc Data Sheet only)

Intelligence Program
DGSTA Defence Intelligence Organisation
Manager, Information Centre, Defence Intelligence Organisation

Corporate Support Program
Library Manager, DLS-Canberra
Ms Sam Doran, Defence Library Service - Sydney West (Doc Data Sheet)

UNIVERSITIES AND COLLEGES
Australian Defence Force Academy
Library
Head of Aerospace and Mechanical Engineering
Serials Section (M list), Deakin University Library, Geelong, VIC
Hargrave Library, Monash University (Doc Data Sheet only)
Librarian, Flinders University

OTHER ORGANISATIONS
NASA (Canberra)
AusInfo

OUTSIDE AUSTRALIA

ABSTRACTING AND INFORMATION ORGANISATIONS
Library, Chemical Abstracts Reference Service
Engineering Societies Library, US
Materials Information, Cambridge Scientific Abstracts, US
Documents Librarian, The Center for Research Libraries, US

INFORMATION EXCHANGE AGREEMENT PARTNERS

Acquisitions Unit, Science Reference and Information Service, UK
Library - Exchange Desk, National Institute of Standards and Technology, US

SPARES (5 copies)

Total number of copies: 63

DEFENCE SCIENCE AND TECHNOLOGY ORGANISATION
DOCUMENT CONTROL DATA

1. PRIVACY MARKING/CAVEAT (OF DOCUMENT)

2. TITLE

A Parametric Study of Jet/Vortex Interactions in the AMRL Water Tunnel

3. SECURITY CLASSIFICATION (FOR UNCLASSIFIED REPORTS THAT ARE LIMITED RELEASE USE (L) NEXT TO DOCUMENT CLASSIFICATION)

Document (U)
Title (U)
Abstract (U)

4. AUTHOR(S)

Lincoln P. Erm

5. CORPORATE AUTHOR

Aeronautical and Maritime Research Laboratory
506 Lorimer St
Fishermans Bend Victoria 3207 Australia

6a. DSTO NUMBER	6b. AR NUMBER	6c. TYPE OF REPORT	7. DOCUMENT DATE
DSTO-TR-1209	AR- 012-017	Technical Report	September 2001

8. FILE NUMBER	9. TASK NUMBER	10. TASK SPONSOR	11. NO. OF PAGES	12. NO. OF REFERENCES
M1/9/358	DST98/129	DSTO	60	12

13. URL on the World Wide Web

http://www.dsto.defence.gov.au/corporate/reports/DSTO-TR-1209.pdf

14. RELEASE AUTHORITY

Chief, Air Operations Division

15. SECONDARY RELEASE STATEMENT OF THIS DOCUMENT

Approved for public release

OVERSEAS ENQUIRIES OUTSIDE STATED LIMITATIONS SHOULD BE REFERRED THROUGH DOCUMENT EXCHANGE, PO BOX 1500, EDINBURGH, SA 5111

16. DELIBERATE ANNOUNCEMENT

No Limitations

17. CITATION IN OTHER DOCUMENTS Yes

18. DEFTEST DESCRIPTORS

F/A-18 aircraft Aircraft control Jet flow Vortices Flow visualization Water tunnels

19. ABSTRACT

In this report, details are given of a parametric study undertaken in the AMRL flow-visualisation water tunnel to determine how vortices are affected when they interact with different types of jet flows. The effects on vortices of jets having different shapes, velocities, locations and pitch angles were investigated. The flow was visualized using dye and vortex behaviour was examined for 42 different jets. It was found that jet shape, jet velocity and jet location all had a significant effect on vortex behaviour, whereas jet pitch angle generally had a minimal effect. Possible physical explanations for vortex behaviour have been proposed. The parametric study is the first stage of a longer investigation aimed at determining the best jet configurations to use to control vortical flow over modern high-performance aircraft to improve aircraft control at extreme flight attitudes. The findings of the initial parametric study will be used in any ongoing work on the investigation.